IJAME

Int. J. of Applied Mechanics and Engineering, 2026, vol.???, No.???, pp.???-???
DOI: 10.59441/ijame/219787

TRANSIENT ELECTRO-MAGNETOHYDRODYNAMIC 2-LIQUID PLASMA FLOW THROUGH A CONDUCTING PERMEABLE CHANNEL WITH HALL EFFECTS

V. Gowri Sankara Rao[1] and T. Linga Raju[2*]
[1]Department of Mathematics, St.Joseph's College for Women(A), Visakhapatnam, A.P., INDIA
E-mail: gowrisankara@stjosephsvizag.com
[2] Department of Engineering Mathematics, AUCE (A), Andhra University, Visakhapatnam, INDIA
E-mail: tlraju45@yahoo.com

Understanding the heat transfer behaviour of electrically conducting gases in magneto hydrodynamic (MHD) systems is crucial for optimizing applications in energy systems, plasma control, and advanced cooling technologies with practical uses in reactor cooling, aerodynamic boundary layer control, spacecraft etc. So, this study investigates the transient two-fluid heat transmission flow of electrically conducting gases driven by a uniform pressure gradient between parallel, permeable plates, aiming to extend existing MHD models by incorporating the combined effects of unsteadiness, Hall currents and wall porosity. The governing partial differential equations are solved using a regular perturbation technique to obtain analytical expressions for velocity and temperature distributions. The results reveal that increasing the Hartmann number and Hall parameter significantly enhances the heat transfer coefficient, with the effect being more pronounced when the channel walls allow electric current conduction. Furthermore, higher wall porosity and favorable ratios of electrical conductivity to fluid viscosity lead to notable alterations in both flow resistance and heat transfer rates. These findings emphasize that the combined effects of magnetic field intensity, Hall currents, and wall porosity characteristics play a pivotal role in controlling unsteady MHD flow and thermal transport in conducting channels.

Key words: Hall effect, MHD heat flow, plasma, two-fluid flow, porous plates (conducting), regular perturbation method.

1. Introduction

Magnetohydrodynamics (MHD) has remarkable significance on fluid flow through straight pipes/parallel plate's geometry. Numerous scientists (Hartmann [1], Siegal [2], Nigam and Singh [3], Alpher [4], Shercliff [5], Singh and Cowling [6], Alireza and Sahai [7], Morley *et al.* [8], Selimli and Resebli [9], Jovanovic *et al.* [10], Hsiao Kai-Long [11], Nikodijevic *et al.* [12], Das *et al.* [13], Sadab and Kundu [14-15]) have done applaud able theoretical and scientific works on the flow induced as a result of the magnetic field in view of its considerable importance in several engineering and industrial disciplines under different assumptions. Owing to their practical importance in engineering and industry, magnetohydrodynamic two-fluid flows through channels, pipes, and tubes have become a topic of considerable research attention. In recent years, an investigation into heat transfer processes within two-phase flow systems under an external magnetic field has garnered significant attention due to its impact on the thermal performance of the numerous engineering and industrial systems. Examples include, electronic cooling, solar receiving systems, energy storage systems. These flows are also significant in the petrochemical industry, particularly in oil production and transportation, and in environmental geothermal systems.

The Hall effect, which occurs when an intense magnetic field interacts under low plasma density conditions, alters ionized gas flow patterns. This effect is relevant in astrophysics like solar flares and magnetospheres, geophysics, aerodynamic heating, plasma control generators, radio wave propagation, MHD

---

[*] To whom correspondence should be addressed

power generators, MHD accelerators, and fusion reactors and Hall accelerators. Also, Hall Effect has applications in spacecraft propulsion, Hall Effect thrusters; create thrust by ionizing and accelerating gas. Though earlier studies overlooked the Hall current's influence, it is then recognized as essential in MHD applications. Many researchers have contributed to understanding Hall currents in MHD flows. The early works of Sherman and Sutton [16], Sato [17], Roming [18] laid the foundation. Subsequently, researchers like Jana and Datta [19], Mabdal and Mandal [20], Sharma and Neela Rani [21], Temburu and RamanaRao [22], Attia [23], Takhar *et al.* [24], Ghosh *et al.* [25], Hazem Ali Attia [26], Jha and Apere [27], Pal *et al.* [28], Sadia Siddia *et al.* [29], Makinde *et al.* [30], Rashidi and Momoniat [31], Gorla and Gupta [32], Das and Deka [33], Alam [34], Matao *et al.* [35], Hossain and Alim [36], Temburu and Satish [37], Ramesh and Ojjela [38] analyzed Hall current effects in MHD flows with different configurations.

The impact of Hall currents on porous boundary flows has been extensively investigated due to its significance in advancing technologies such as nuclear reactors, energy conversion systems, catalytic converters, power generation, heat exchangers, electronic cooling systems, radiators, energy storage systems, plasma studies, and aerospace applications. Notable contributions in this area include the works of Shrestha [39], Ockendon and Ockendon [40], Debnath *et al.* [41], Attia and Sayed-Ahmed [42], Attia [43], Ganesh and Krishnambal [44], Ahmed and Goswami [45], Manyonge *et al.* [46], Das *et al.* [47], Jaber [48], Singh *et al.* [49], Akinshilo Akinbowale [50] and Veera Krishna *et al.* [51], Nayak *et al.* [52], Vangala and Temburu [53].

Magnetohydrodynamic (MHD) two-phase flows have been extensively studied, with researchers examining various thermal and flow characteristics in the existence of magnetic fields. Lohrasbi and Sahai [54] analyzed the effects of temperature-dependent transport properties. In their study, Malashetty and Leela [55] analyzed MHD heat transfer in two-fluid systems. In contrast, Chamkha [56] investigated the transient behavior of MHD-driven heat and mass transfer in a porous structure. Further contributions by Sharma and Rani [57-58] and Temburu and Sreedhar [59] addressed ionized fluid heat transfer and flow behavior in the existence of a transverse magnetic field, enhancing applications in plasma physics, industrial processes, and space technology -particularly valuable for optimizing energy extraction in nuclear and geothermal power plants. Additional notable studies in this area include those by Kalra *et al.* [60], Packham and Sail [61], Shail [62], Shikhmurzaev [63], Vajravelu *et al.* [64], Umavathi *et al.* [65], Ozen *et al.* [66], Murthy and Srinivas [67], Temburu and Naga Valli [68], Sharma and Sharma [69], Sivakamini and Govindarajan [70], AbdElmaboud *et al.* [71], Roy and Shaw [72] Temburu and Satish [73], Temburu and Naga Valli [74].

The growing innovation in modern mechanism has intensified research exploring the dynamics of MHD multi-fluid flow systems, owing to their wide-ranging industrial and engineering applications. A clear understanding of thermal convection and fluid thermal behavior in dual-phase flow models is essential for the development of devices such as thermonuclear reactors, conductive fluid power generation systems, and magnetic induction pumps. In geothermal regions, using two-fluid flow models in electromagnetic pumps improves flow rates and reduces power consumption in oil transportation. The transient nature of fluid flows, especially in immiscible fluids, presents challenges in petroleum, geophysics, and magneto-fluid dynamics. Hall currents, significant in astrophysical and plasma physics applications, impact unsteady MHD two-fluid flow, requiring further investigation.

Although considerable research has been conducted on magnetohydrodynamic flows, studies specifically addressing dual-fluid MHD systems examined with and without Hall current contributions remain relatively scarce. Kalra *et al.* [75] investigated the effects of Hall currents and electrical resistivity in gas-liquid systems. Relevant investigations in this direction include works by Temburu [76], Srinivasacharya and Kaladhar [77], yet most existing work has primarily concentrated on steady-state conditions. This work explores an important yet less-studied aspect of magnetohydrodynamic (MHD) flows–the combined effects of Hall currents and wall porosity in unsteady two-fluid systems. While most earlier studies focus on steady-state or single-fluid cases, so this article investigates transient, immiscible conducting fluids moving between a horizontal channel consisting of electrically conductive, permeable side plates under the influence of a transverse magnetic field. Using a regular perturbation method, it provides approximate analytical solutions for velocity and temperature, showing how Hartmann number, Hall parameter, and porous boundaries together influence heat transfer and flow resistance. A unique contribution is the comparison between zero-ionization and partial-ionization cases, highlighting the role of electron pressure fraction. These insights can be applied in advanced systems such as nuclear reactor cooling, and aerospace thermal protection, plasma propulsion, MHD power generation, and offers valuable guidance for designing high-performance thermal and fluid control technologies.

2. Analytical derivation and mathematical analysis of the problem

The main aim of the present investigation is to examine the behavior of a magneto hydrodynamic two-phase flow system, where electrically charged gases are driven through a horizontal flow conduit under the in significance of a uniform pressure gradient denoted by ($-\frac{\partial p}{\partial x}$). The setup operates under the significance of externally magnetic and electric fields exerted perpendicular to the flow direction, considering the flow as time-dependent, smooth, and fully established. The analysis is carried out based on the following considerations:

- The model considers a horizontal flow channel situated between two parallel walls of infinite length in the x and z directions.
- A rectangular (Cartesian) coordinate framework is adopted, placing the origin midway between the channel walls. The pressure gradient is directed parallel to the x-axis, which extends along the channel walls but does not always match the actual flow direction.
- It is assumed that the channel's width is substantially greater than its height to simplify the flow analysis.
- The channel walls are electrically conducting and maintained at constant but different temperatures, represented by T_{w1} at $y = h_1$ and T_{w2} at $y = h_2$ the upper portion of the channel is referred to as region-I, and the bottom fluid region, referred to as region-II, covering the ranges from $0 \le y \le h_1$ and $-h_2 \le y \le 0$ respectively.
- The two fluid domains are considered non-miscible, electrically conducting, and volume-conserving, each characterized by unique physical properties, including varying densities: ρ_1, ρ_2, viscosities: μ_1, μ_2, electrical conductivities: σ_{01}, σ_{02}, and thermal conductivities: K_1, K_2.
- A constant, uniform magnetic field 'B_0' is applied perpendicular to the channel walls along the y-axis, with the effects of Hall currents being considered in the analysis.
- Induced magnetic effects are disregarded under the assumption of a low magnetic Reynolds number.
- Boundary layer between the fluids separating the two-layer fluid system is presumed to be uniform, free from shear stress, and stable throughout the flow domain to maintain the integrity of the boundary.

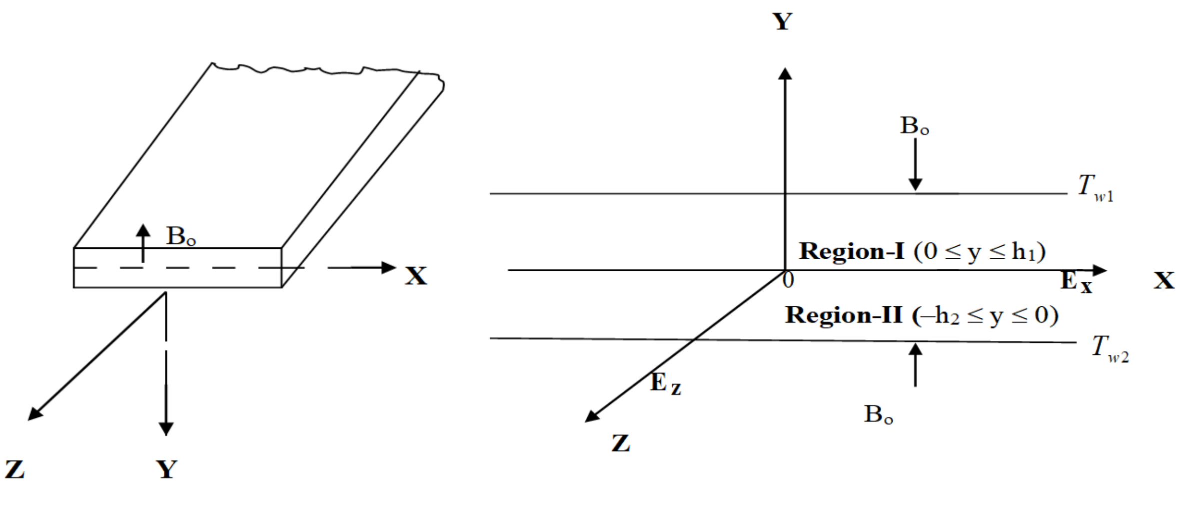

Fig.A. Flow scheme in coordinates.

- Consistent temperature conditions are enforced at the channel walls, assuming heat conduction happens solely along the flow path and ignoring the contribution of electron heating.
- Since the plates extend infinitely in the x- and z-directions, all flow variables, except for pressure, depend only on the y-direction and time 't'.

Based on the aforementioned assumptions and guided by insights from established research, the fundamental flow equations are developed to depict the time-dependent MHD flow and associated heat flow inside a channel formed by parallel conducting boundaries. The system is influenced by externally applied transverse electric and magnetic fields and consists of two immiscible, electrically conducting fluid layers. These governing equations are derived based on the core laws of fluid motion governing the unsteady behavior of fully ionized, electrically neutral plasma, with explicit consideration given due to the presence of Hall effects.

The theoretical study incorporates the momentum, current continuity, and energy equations, tailored for unsteady fluid motion. Appropriate boundary and interfacial conditions are applied to capture the physical behavior at the channel walls and at the interface separating the two fluid layers. This formulation builds upon and extends classical studies on hydromagnetic steady flows, particularly the foundational contributions of Sato [17], Temburu [76], Spitzer [78], Nayak *et al.* [79] and Sadab and Kundu [80].

Governing equations of motion:

$$\rho\left[\frac{\partial \overline{V}}{\partial t}+\left(\overline{V}.\nabla\right)\overline{V}\right]=-\nabla p+\mu\nabla^{2}\overline{V}+\left(\overline{J}\times\overline{B}\right). \tag{2.1}$$

Current equation:

$$\overline{E}+\overline{V}\ x\ \overline{B}\ +\ \overline{E_e}-\frac{c}{en}\ \overline{J}\ x\ \overline{B}-\frac{\overline{J}}{\sigma_0}=0\,. \tag{2.2}$$

Energy conservation equation:

$$\rho\, c_p\left(\frac{\partial T}{\partial t}+\left(\overline{V}.\nabla\right)T\right)=K\ \nabla^{2}\ T\ +\ \phi+\left(\overline{J}^{2}\ /\ \sigma_0\right). \tag{2.3}$$

Continuity equation for incompressible fluid flow:

$$\nabla.\overline{V}=0\,. \tag{2.4}$$

The fundamental equations governing the behaviour of fluid motion and electrical current in time-dependent magneto hydrodynamic flow behaviour of a fully ionized, electrically neutral fluid within a two-layer fluid system confined between two parallel, porous channel walls are developed based on the theoretical frameworks established by Sato [17], Spitzer [78], Malashetty and Leela [55] and Temburu and Valli [74]. These equations, applicable to both fluid regions, provide a comprehensive framework for analyzing the dynamics of the system. We examine the two-fluid regions by considering key physical parameters, considering the velocity distribution $\overline{V_i}=(u_i,0,w_i)$, magnetic flux $\overline{B}=(0,\ B_0,0)$, current intensity $\overline{J_i}=(J_{ix},0,J_{iz})$, and electric field strength $\overline{E_i}=(E_{ix},0,E_{iz})$ with specified vector components, and by incorporating the relation $J_i^2=J_{ix}^2+J_{iz}^2,\,(i=1,2)$ the governing set of equations capturing the flow dynamics and electromagnetic responses in both the upper and lower fluid domains (Region-I and Region-II) are systematically derived and expressed as follows:

Region-I:

$$\rho_1 \frac{\partial u_1}{\partial t} = \rho_1 \nu_1 \frac{\partial^2 u_1}{\partial y^2} - \rho_1 v_0 \frac{\partial u_1}{\partial y} - \left\{ 1 - s\left[1 - \frac{\sigma_{11}}{\sigma_{01}} \right] \right\} \frac{\partial p}{\partial x} + \\ + \left\{ -\sigma_{11}\left[E_{1z} + u_1 B_0 \right] + \sigma_{21}\left[E_{1x} - w_1 B_0 \right] \right\} B_0, \tag{2.5}$$

$$\rho_1 \frac{\partial w_1}{\partial t} = \rho_1 \nu_1 \frac{\partial^2 w_1}{\partial y^2} - \rho_1 v_0 \frac{\partial w_1}{\partial y} + \left(s \frac{\sigma_{21}}{\sigma_{01}} \right) \frac{\partial p}{\partial x} + \left\{ \sigma_{11}(E_{1x} - w_1 B_0) + \sigma_{21}\left[E_{1z} + u_1 B_0 \right] \right\} B_0, \tag{2.6}$$

$$\rho_1 c_{p_1} \frac{\partial T_1}{\partial t} = \frac{c_{p_1}\mu_1}{P_r} \frac{\partial^2 T_1}{\partial y^2} + \rho_1 v_0 \frac{\partial T_1}{\partial y} + \mu_1 \left[\left(\frac{\partial u_1}{\partial y} \right)^2 + \left(\frac{\partial w_1}{\partial y} \right)^2 \right] + \frac{J_1^2}{\sigma_{01}}, \tag{2.7}$$

$$J_{1x} = \sigma_{11} E_{1x} - B_0 \sigma_{11} w_1 + \sigma_{21} E_{1z} + B_0 \sigma_{21} u_1 + \frac{s\sigma_{21}}{\sigma_{01} B_0} \left(\frac{\partial p}{\partial x} \right), \tag{2.8}$$

$$J_{1z} = \sigma_{11} \left(\frac{E_{1z}}{B_0} + u_1 \right) - \sigma_{21} \left(\frac{E_{1x}}{B_0} - w_1 \right) - \frac{s}{B_0} \left(1 - \frac{\sigma_{11}}{\sigma_{01}} \right) \left(\frac{\partial p}{\partial x} \right) \tag{2.9}$$

Region-II:

$$\rho_2 \frac{\partial u_2}{\partial t} = \rho_2 \nu_2 \frac{\partial^2 u_2}{\partial y^2} - \rho_2 v_0 \frac{\partial u_2}{\partial y} - \left\{ 1 - s\left[1 - \frac{\sigma_{12}}{\sigma_{02}} \right] \frac{\partial p}{\partial x} \right\} + \\ + \left\{ -\sigma_{12}[E_{2z} + u_2 B_0] + \sigma_{22}[E_{2x} - w_2 B_0] \right\} B_0, \tag{2.10}$$

$$\rho_2 \frac{\partial w_2}{\partial t} = \rho_2 \nu_2 \frac{\partial^2 w_2}{\partial y^2} - \rho_2 v_0 \frac{\partial w_2}{\partial y} + \left(s \frac{\sigma_{22}}{\sigma_{02}} \right) \frac{\partial p}{\partial x} + \left\{ \sigma_{12}(E_{2x} - w_2 B_0) + \sigma_{22}(E_{2z} + u_2 B_0) \right\} B_0, \tag{2.11}$$

$$\rho_2 c_{p_2} \frac{\partial T_2}{\partial t} = \frac{c_{p_2}\mu_2}{P_r} \frac{\partial^2 T_2}{\partial y^2} + \rho_2 v_0 \frac{\partial T_2}{\partial y} + \mu_2 \left\{ \left[\frac{\partial u_2}{\partial y} \right]^2 + \left[\frac{\partial w_2}{\partial y} \right]^2 \right\} + \frac{J_2^2}{\sigma_{02}}, \tag{2.12}$$

$$J_{2x} = (\sigma_{12} E_{2x}) - (B_0 \sigma_{12} w_2) + (\sigma_{22} E_{2z}) + (B_0 \sigma_{22} u_2) + \frac{s\sigma_{22}}{\sigma_{02} B_0} \left(\frac{\partial p}{\partial x} \right), \tag{2.13}$$

$$J_{2z} = \sigma_{12} E_{2z} + \sigma_{12} B_0 u_2 - \sigma_{22} E_{2x} + \sigma_{22} B_0 w_2 - \frac{s}{B_0} \left(1 - \frac{\sigma_{12}}{\sigma_{02}} \right) \left(\frac{\partial p}{\partial x} \right). \tag{2.14}$$

In the developed system of equations, subscripts 1 and 2 are employed to differentiate the corresponding physical parameters in Region-I and Region-II. The velocity components u_1, u_2 and w_1, w_2 represent the fluid flow rates in the x- and z-directions, respectively, for each fluid layer, signifying the primary and secondary velocity profiles. Similarly, the symbols E_{ix} and E_{iz} , J_{ix} and J_{iz} $(i = 1,2)$ denote the respective components of the electric field strength and current density vectors along the x- and z-axes in both fluid domains. The temperatures in Region-I and Region-II are denoted by T_1 and T_2, respectively $c_{pi}(i=1,2)$ denotes the specific heat of the fluids at constant pressure.

A non-dimensional indicator, denoted as 's', is defined as electron-to-total pressure ratio $(s = p_e / p)$ within the plasma medium. A value of $s = 1/2$ represents a fully ionized, neutral plasma, whereas values approaching zero indicate a weakly ionized gaseous state. The coefficients σ_{11}, σ_{12} and σ_{21}, σ_{22} represent refined electrical conductivities, oriented either parallel or perpendicular to the electric field, depending on their respective definitions. As the top and bottom walls of the channel are sustained at uniform temperatures T_{w1} and T_{w2}, the associated temperature-dependent functions $\frac{\partial T_1}{\partial x}=0, \frac{\partial T_1}{\partial z}=0, \frac{\partial T_2}{\partial x}=0, \frac{\partial T_2}{\partial z}=0$ and T_1, T_2 are assumed to be finite and vary solely with respect to the y-coordinate and time 't' within the two-fluid domains. The interface located at $y=0$ ensures the continuity of both fluid velocities and tangential shear stresses. Furthermore, isothermal boundary conditions are applied at the channel walls, maintaining not only consistent temperature values but smooth conduction of heat through the interface dividing the two fluids.

The specified velocity constraints at both boundaries and interfaces in the flow system are:

$$u_1(h_1) \text{ and } w_1(h_1) = \begin{cases} 0 & \text{for } \ t \le 0, \\ \text{real of } \varepsilon e^{i\omega t} & \text{for } \ t > 0, \end{cases} \tag{2.15}$$

$$u_2(-h_2) = 0, \ \ w_2(-h_2) = 0, \tag{2.16}$$

At the interface between the two regions $u_1(0) = u_2(0)$, $w_1(0) = w_2(0)$ (2.17)

$$\mu_1\left[\frac{\partial u_1}{\partial y}\right] = \mu_2\left[\frac{\partial u_2}{\partial y}\right] \text{ and } \mu_1\left(\frac{\partial w_1}{\partial y}\right) = \mu_2\left(\frac{\partial w_2}{\partial y}\right) \text{ at } y=0. \tag{2.18}$$

Temperature boundary and transition conditions for the fluid domains:

$$\begin{gathered} T_1[h_1] = T_{w1}, \ T_2[-h_2] = T_{w2}, \ T_1[0] = T_2[0] \text{ at interface,} \\ K_1\left(\frac{\partial T_1}{\partial y}\right) = K_2\left(\frac{\partial T_2}{\partial y}\right) \text{ at } y=0. \end{gathered} \tag{2.19}$$

The equations numbered (2.5) to (2.14) and (2.15) to (2.19) are expressed in non-dimensional form using these parameters:

$$u_1^* = \frac{u_1}{u_p}, \quad u^*_2 = \frac{u_2}{u_p}, \quad w^*_1 = \frac{w_1}{u_p}, \quad w^*_2 = \frac{w_2}{u_p}, \quad y^*_i = \frac{y_i}{h_i}, \quad u_p = -\frac{\partial p}{\partial x}\frac{h_1^2}{\mu_1},$$

$$t^* = \frac{\mu_i t}{\rho_i h_i^2}, \quad \omega^* = \frac{\omega h_i^2 \rho_i}{\mu_i} \ (i=1,2), \quad m_{ix} = \frac{E_{ix}}{B_0 u_p}, \quad m_{iz} = \frac{E_{iz}}{B_0 u_p},$$

$$I_{ix} = \frac{J_{ix}}{\sigma_{0i} B_0 u_p}, \quad I_{iz} = \frac{J_{iz}}{\sigma_{0i} B_0 u_p}, \quad J_i^2 = J_{ix}^2 + J_{iz}^2,$$

$$M \text{ (Hartmann number)} = B_0 h_1 \sqrt{\left(\frac{\sigma_{01}}{\mu_1}\right)}, \qquad \alpha \text{ (The viscosity ratios)} = \frac{\mu_1}{\mu_2},$$

$$h \text{ (the height ratios)} = \frac{h_2}{h_1}, \qquad \rho \text{ (The density ratios)} = \frac{\rho_2}{\rho_1},$$

$$\sigma_0 \text{ (conductivity ratio of the two media)} = \frac{\sigma_{01}}{\sigma_{02}}, \qquad \lambda \text{ (porous parameter)} = \frac{Lv_0}{\upsilon},$$

$$\sigma_{01} = \frac{\sigma_{12}}{\sigma_{11}}, \quad \sigma_{02} = \frac{\sigma_{22}}{\sigma_{21}}, \quad \frac{\sigma_{11}}{\sigma_{01}} = \frac{1}{1+m^2}, \quad \frac{\sigma_{21}}{\sigma_{01}} = \frac{m}{1+m^2}, \quad m \text{ (Hall parameter)} = \frac{\omega_e}{\left(\frac{1}{\tau} + \frac{1}{\tau_e}\right)},$$

$$\beta \text{ (ratio of heat conductivities in the both fluid regions)} = \frac{K_1}{K_2},$$

$$\theta_i \text{ (distribution of temperature)} = \frac{T_i - T_{wi}}{\left(u_p{}^2 \mu_1 / K_i\right)}. \tag{2.20}$$

Here, ω_e refers to the angular motion frequency of electrons, while τ and τ_e indicate the characteristic interaction times energy transfer events between electrons, ions, and neutral gas constituents. The Hall parameter 'm', which characterizes partially ionized gases, converges to the expression used for totally ionized fluid as the temperature τ_e increases indefinitely, ε is amplitude, typically representing a small constant value, $\varepsilon << 1$. The symbol λ is the suction parameter, also known as the suction number or porous parameter (a dimensionless quantity that represents the ratio of suction velocity to a characteristic flow velocity). It is expressed as $\lambda = \frac{Lv_0}{\upsilon}$, where v_0 denotes the suction velocity. This parameter is often used to describe the influence of fluid removal or injection through a porous boundary on the overall flow behavior.

Boundary conditions:

For viscous fluids, the movement at the boundary follows the no-slip condition, meaning the fluid in direct contact with a rigid surface matches the velocity of that surface. If the boundary is fixed, the velocity at the wall is zero, while for a moving plate; it equals the plate's velocity. This rule applies similarly to other velocity components such as 'v' and 'w'. At the interface between two immiscible fluids, both velocity and shear stress are assumed to remain continuous across the boundary.

In terms of heat transfer, isothermal boundary conditions are often applied, assuming the solid surfaces in contact with the fluid have infinite thermal conductivity and heat capacity. Under these conditions, the fluid temperature at the surface matches that of the boundary. At interfaces between two immiscible fluids, both temperature and heat flux are considered continuous, ensuring smooth thermal behavior across the junction.

By implementing the variable substitutions outlined in Eq.(2.20) and omitting the asterisk notations for simplicity, Eqs (2.5) to (2.14) are reformulated into their dimensionless counterparts. Moreover, it is assumed that the channel's lateral plates, constructed from electrically responsive material and interconnected via an external conductive channel, allow the generated electric currents to exit the channel. This configuration ensures that no electrical potential imbalance is present across the channel walls. Additionally, assigning the values $m_x = 0$, $m_z = 0$ eliminates the electrical intensity components in the x- and z-directions, consistent with the assumptions made by Sato [17], Temburu [76] and Temburu and Venkat [81]. Under these conditions, the final dimensionless flow equations for fluid motion, electric current, heat transfer, and associated boundary conditions in both fluid domains are established. In the following equations, the ‘*’ symbol has been omitted for simplicity, since all variables are already represented in their non-dimensional form based on the defined parameters.

Region-I:

$$\frac{\partial u_1}{\partial t}+\lambda\frac{\partial u_1}{\partial y}=\frac{\partial^2 u_1}{\partial y^2}-\left(\frac{M^2}{1+m^2}\right)\left(m_{z_1}+u_1\right)+\left(\frac{mM^2}{1+m^2}\right)\left(m_{x_1}-w_1\right)+k_1, \tag{2.21}$$

$$\frac{\partial w_1}{\partial t}+\lambda\frac{\partial w_1}{\partial y}=\frac{\partial^2 w_1}{\partial y^2}+\left(\frac{M^2}{1+m^2}\right)\left(m_{x_1}-w_1\right)+\left(\frac{mM^2}{1+m^2}\right)\left(m_{z_1}+u_1\right)+k_2, \tag{2.22}$$

$$\frac{\partial \theta_1}{\partial t}=\frac{1}{P_r}\frac{\partial^2 \theta_1}{\partial y^2}+\lambda\frac{\partial \theta_1}{\partial y}+\left\{\left(\frac{\partial \mathrm{u}_1}{\partial \mathrm{y}}\right)^2+\left(\frac{\partial w_1}{\partial y}\right)^2+M^2 I_1^{\,2}\right\}, \tag{2.23}$$

$$I_{1x}=\left(\frac{1}{1+m^2}\right)\left(m_{x_1}-w_1\right)+\left(\frac{m}{1+m^2}\right)\left(m_{z_1}+u_1\right)-\frac{s}{M^2}\left[\frac{m}{1+m^2}\right], \tag{2.24}$$

$$I_{1z}=\left(\frac{1}{1+m^2}\right)\left(m_{z_1}+u_1\right)-\left(\frac{m}{1+m^2}\right)\left(m_{x_1}-w_1\right)+\frac{s}{M^2}\left[1-\frac{m}{1+m^2}\right], \tag{2.25}$$

$$I_1^2=I_{1x}^{\,2}+I_{1z}^{\,2}.$$

Region-II:

$$\begin{aligned}\frac{\partial u_2}{\partial t}+\rho\alpha h\lambda\frac{\partial u_2}{\partial y}=\frac{\partial^2 u_2}{\partial y^2}-\left(\frac{1}{1+m^2}\right)\alpha\sigma_1 h^2 M^2\left(m_{z_2}+u_2\right)+\\+\left(\frac{m}{1+m^2}\right)\alpha\sigma_2 h^2 M^2\left(m_{x_2}-w_2\right)+\beta_1\alpha h^2,\end{aligned} \tag{2.26}$$

$$\begin{aligned}\frac{\partial w_2}{\partial t}+\rho\alpha h\lambda\frac{\partial w_2}{\partial y}=\frac{\partial^2 w_2}{\partial y^2}+\left(\frac{1}{1+m^2}\right)\alpha\sigma_1 h^2 M^2\left(m_{x_2}-w_2\right)+\\+\left(\frac{m}{1+m^2}\right)\alpha\sigma_2 h^2 M^2\left(m_{z_2}+u_2\right)+\beta_2\alpha h^2,\end{aligned} \tag{2.27}$$

$$\frac{\partial \theta_2}{\partial t}=\frac{1}{P_r}\frac{\partial^2 \theta_2}{\partial y^2}+\lambda\frac{\partial \theta_2}{\partial y}+\frac{\beta}{\alpha}\left[\left(\frac{\partial \mathrm{u}_2}{\partial \mathrm{y}}\right)^2+\left(\frac{\partial w_2}{\partial y}\right)^2\right]+\beta\sigma h^2 M^2 I_2^{\,2}, \tag{2.28}$$

$$I_{2x}=\left(\frac{\sigma_0\sigma_{01}}{1+m^2}\right)\left(m_{x_2}-w_2\right)+\left(\frac{m\sigma_0\sigma_{02}}{1+m^2}\right)\left(m_{z_2}+u_2\right)-\frac{s\sigma_0^{\,2}\sigma_{02}}{M^2}\left(\frac{m}{1+m^2}\right), \tag{2.29}$$

$$I_{2z}=\left(\frac{\sigma_0\sigma_{01}}{1+m^2}\right)\left(m_{z_2}+u_2\right)-\left(\frac{m\sigma_0\sigma_{02}}{1+m^2}\right)\left(m_{x_2}-w_2\right)+\frac{s\sigma_0}{M^2}\left(1-\frac{\sigma_0\sigma_{01}}{1+m^2}\right), \tag{2.30}$$

$$I_2^{\,2}=I_{2x}^{\,2}+I_{2z}^{\,2}$$

where, $\beta_1=1-s\left(\dfrac{1}{1+m^2}\right)$, $\beta_2=\dfrac{-sm}{1+m^2}$, $\beta_3=1-s\left(1-\dfrac{\sigma_0\sigma_{01}}{1+m^2}\right)$, $\beta_4=\dfrac{-s\sigma_0\sigma_{02}m}{1+m^2}$.

Conditions at the boundaries and interface for the velocity fields u_1, w_1 and u_2, w_2:

$$u_1(1)=\begin{cases}0 & \text{for } t\le 0,\\ \varepsilon\cos\omega t & \text{for } t>0\end{cases} \quad\text{and}\quad w_1(1)=\begin{cases}0 & \text{for } t\le 0,\\ \varepsilon\cos\omega t & \text{for } t>0,\end{cases} \tag{2.31}$$

$$u_2(-1)=0,\quad w_2(-1)=0, \tag{2.32}$$

$$u_1(0)=u_2(0),\quad w_1(0)=w_2(0), \tag{2.33}$$

$$\frac{\partial u_1}{\partial y}=\left[\frac{1}{\alpha h}\right]\frac{\partial u_2}{\partial y},\quad \frac{\partial w_1}{\partial y}=\left[\frac{1}{\alpha h}\right]\frac{\partial w_2}{\partial y}\quad\text{and}\quad \mu_1\frac{\partial w_1}{\partial y}=\mu_2\frac{\partial w_2}{\partial y}\quad\text{at}\quad y=0. \tag{2.34}$$

Temperature boundary conditions and interface constraints for both fluids

$$\theta_1(1)=0,\quad \theta_2(-1)=0,\quad \theta_1(0)=\theta_2(0)\quad\text{and}\quad \frac{\partial\theta_1}{\partial y}=\frac{1}{\beta h}\frac{\partial\theta_2}{\partial y}\quad\text{at}\quad y=0. \tag{2.35}$$

3. Solution methodology

The objective of this research is to obtain solutions for the momentum and heat transfer Eqs (2.21, 2.22, 2.23, 2.26, 2.27 and 2.28) by incorporating the corresponding conditions at the boundaries and interfaces (2.31 to 2.35) are applied to examine the flow speed and thermal distribution across flow regions. The governing equations constitute a coupled set of intricate fluid flow equations that cannot be solved precisely using direct analytical techniques. To address this, a first-order regular perturbation technique is employed, assuming a two-term series approximation, which transforms the system into a set of linear ordinary differential equations.

$$\begin{aligned}&u_1(y,t)=u_{01}(y)+\text{real of }\varepsilon e^{i\omega t}u_{11}(y),\\ &\qquad\qquad\qquad\qquad\text{for } t>0,\\ &w_1(y,t)=w_{01}(y)+\text{real of }\varepsilon e^{i\omega t}w_{11}(y),\end{aligned} \tag{3.1}$$

$$\begin{aligned}&u_2(y,t)=u_{02}(y)+\text{real of }\varepsilon e^{i\omega t}u_{12}(y),\\ &\qquad\qquad\qquad\qquad\text{for } t>0,\\ &w_2(y,t)=w_{02}(y)+\text{real of }\varepsilon e^{i\omega t}w_{12}(y),\end{aligned} \tag{3.2}$$

$$\theta_1(y,t)=\theta_{01}(y)+\text{real of } \varepsilon e^{i\omega t}\ \theta_{11}(y),$$
$$\text{for } t>0. \tag{3.3}$$
$$\theta_2(y,t)=\theta_{02}(y)+\text{real of } \varepsilon e^{i\omega t}\ \theta_{12}(y),$$

Within this framework, the variables '$u_{01}(y)$, $u_{02}(y)$; $w_{01}(y), w_{02}(y)$ and $\theta_{01}(y),\theta_{02}(y)$' denote the steady-state components of velocity and temperature variations across both fluid domains. In contrast, $u_{11}(y), u_{12}(y)$; $w_{11}(y), w_{12}(y)$ and $\theta_{11}(y)$, $\theta_{12}(y)$ represent the unsteady or time-varying parameters, which are essential for analyzing the transient behavior of the system. To streamline the governing Eqs (2.21) and (2.22) are combined into a single expression by introducing a complex-valued function: $q_1(y,t)=u_1(y,t)+i\,w_1(y,t)$. Similarly, Eqs (2.26) and (2.27) are unified by defining $q_2(y,t)=u_2(y,t)+i\,w_2(y,t)$. The relations from Eqs (3.1-3.3) are substituted into Eqs (2.21-2.23) and (2.26-2.28), after which the steady and fluctuating terms are separated to simplify the analysis, a set of differential equations is formulated in terms of complex variables 'q_{01}, q_{11}, q_{02} and q_{12}'. Additional parameters '$q_{01}=u_{01}+iw_{01}$; $q_{11}=u_{11}+iw_{11}$; $q_{02}=u_{02}+iw_{02}$; $q_{12}=u_{12}+iw_{12}$'are also introduced to complete the formulation.

Evaluation of Region-I in steady state

$$\frac{d^2q_{01}}{dy^2}-\lambda\frac{dq_{01}}{dy}+c_1q_{01}=c_2, \tag{3.4}$$

$$\begin{aligned}\frac{d^2\theta_{01}}{dy^2}+\lambda\frac{d\theta_{01}}{dy}&=-d_{27}e^{d_{23}y}-d_{28}e^{d_{24}y}-d_{29}e^{d_{25}y}-d_{30}e^{d_{26}y}+\\&-d_{31}e^{f_{30}y}-d_{32}e^{f_{31}y}-d_{33}e^{\overline{f_{30}}y}-d_{34}e^{\overline{f_{31}}y}-d_{35}.\end{aligned} \tag{3.5}$$

In the case of time-dependent transient flow

$$\frac{d^2q_{11}}{dy^2}-\lambda\frac{dq_{11}}{dy}+\left(c_1+\omega\tan\omega t\right)q_{11}=0, \tag{3.6}$$

$$\begin{aligned}\frac{d^2\theta_{11}}{dy^2}+\lambda\frac{d\theta_{11}}{dy}+d_{120}\theta_{11}&=d_{142}e^{d_{138}y}+d_{143}e^{d_{139}y}+d_{144}e^{d_{140}y}+\\&+d_{145}e^{d_{141}y}+d_{136}e^{f_{34}y}+d_{137}e^{f_{35}y}+d_{134}e^{\overline{f_{34}}\,y}+d_{135}e^{\overline{f_{35}}\,y}.\end{aligned} \tag{3.7}$$

Evaluation of Region-II in steady state

$$\frac{d^2q_{02}}{dy^2}-\lambda\frac{dq_{02}}{dy}+c_3q_{02}=c_4, \tag{3.8}$$

$$\begin{aligned}\frac{d^2\theta_{12}}{dy^2}+h\rho\alpha\lambda\frac{d\theta_{12}}{dy}+d_{120}\theta_{12}&=-d_{78}e^{d_{74}y}-d_{79}e^{d_{75}y}-d_{80}e^{d_{76}y}+\\&-d_{81}e^{d_{77}y}-d_{82}e^{f_{32}y}-d_{83}e^{f_{33}y}-b_{84}e^{\overline{f_{32}}y}-b_{85}e^{\overline{f_{33}}y}-d_{73}.\end{aligned} \tag{3.9}$$

In the case of time-dependent transient flow

$$\frac{d^2 q_{12}}{dy^2} - \lambda \frac{dq_{12}}{dy} + \left(c_3 + \omega \tan \omega t\right) q_{12} = 0\,, \tag{3.10}$$

$$\begin{gathered}\frac{d^2\theta_{12}}{dy^2} + h\rho\alpha\lambda\frac{d\theta_{12}}{dy} + d_{120}\theta_{12} = d_{189}e^{d_{185}y} + d_{190}e^{d_{186}y} + d_{191}e^{d_{187}y} + \\ + d_{192}e^{d_{188}y} + d_{183}e^{f_{36}y} + d_{184}e^{f_{37}y} + d_{181}e^{\overline{f_{36}}y} + d_{182}e^{\overline{f_{37}}y}\,.\end{gathered} \tag{3.11}$$

Conductive plates: a case analysis:

When the lateral boundaries are composed of electrically conducting substances and are interconnected by an external electrical conduit, the induced current is allowed to flow beyond the channel walls. Under these circumstances, no electric field potential difference is established across the sidewalls. Additionally, by considering the electric field along the *x*- and *z*-directions to be absent, the parameters m_x and m_z are taken as zero, in accordance with the approach by Sato [17]. The constants characterizing the system are then evaluated based on these assumptions. Subsequently, the expressions for the variables u_1, u_2; w_1, w_2; u_{m_1}, u_{m_2}; w_{m_1}, w_{m_2}, I_1 and I_2 within both regions are obtained as follows:

Steady-state analysis in Region-I

$$q_{01}(y) = u_{01}(y) + iw_{01}(y) = f_1 e^{f_{30}y} + f_2 e^{f_{31}y} + \frac{c_2}{c_1}\,, \tag{3.12}$$

In the transient time-dependent component

$$q_{11}(y) = u_{11}(y) + iw_{11}(y) = f_5 e^{f_{34}y} + f_6 e^{f_{35}y}\,, \tag{3.13}$$

$$I_1 = I_{1x} + iI_{1z} = \left[\frac{1}{1+m^2}\right]\left(iu_1 - w_1\right) + \left[\frac{m}{1+m^2}\right]\left(u_1 + iw_1\right) - \frac{s}{M^2}\left\{\frac{m}{1+m^2} - i\left[1 - \frac{m}{1+m^2}\right]\right\}, \tag{3.14}$$

$$\begin{gathered}q_1(y,\,t) = q_{01}(y) + \varepsilon\cos\omega t\,.\,q_{11}(y) = \\ = f_1 e^{f_{30}y} + f_2 e^{f_{31}y} + \frac{c_2}{c_1} + \varepsilon\cos\omega t\left(f_5 e^{f_{34}y} + f_6 e^{f_{35}y}\right).\end{gathered} \tag{3.15}$$

Expression for the mean velocity in complex form

$$q_{m_1} = u_{m_1} + iw_{m_1} = \int_0^1 q_1 dy = f_1 c_{97} + f_2 c_{98} + \frac{c_2}{c_1} + f_{28}\,. \tag{3.16}$$

Steady-state analysis in Region-II

$$q_{02}(y) = u_{02}(y) + iw_{02}(y) = f_3 e^{f_{32}y} + f_4 e^{f_{33}y} + \frac{c_4}{c_3}\,. \tag{3.17}$$

In the transient time-dependent component

$$q_{12}(y) = u_{12}(y) + iw_{12}(y) = f_7 e^{f_{36} y} + f_8 e^{f_{37} y}, \tag{3.18}$$

$$I_2 = I_{2x} + iI_{2z} = \left(\frac{\sigma_0 \sigma_{01}}{1+m^2}\right)(iu_2 - w_2) + \left(\frac{m\sigma_0 \sigma_{02}}{1+m^2}\right)(u_2 + iw_2) + \\ -\frac{s\sigma_0^2 \sigma_{02}}{M^2}\left(\frac{m}{1+m^2}\right) + \frac{s\sigma_0 i}{M^2} - \frac{s\sigma_0^2 \sigma_{01} i}{\left(1+m^2\right)M^2}, \tag{3.19}$$

$$q_2(y,t) = q_{02}(y) + \varepsilon \cos\omega t .\ q_{12}(y) = \\ = f_3 e^{f_{32} y} + f_4 e^{f_{33} y} + \frac{c_4}{c_3} + \varepsilon \cos\omega t\left(f_7 e^{f_{36} y} + f_8 e^{f_{37} y}\right). \tag{3.20}$$

The mean velocity is given by:

$$q_{m_2} = u_{m_2} + iw_{m_2} = \int_0^1 q_2 dy = f_3 c_{99} + f_4 c_{100} + \frac{c_4}{c_3} + f_{29}. \tag{3.21}$$

Conducting plates: temperature variation study:

Derived energy equations applicable to this case

Region-I

$$\frac{\partial \theta_1}{\partial t} = \frac{1}{p_r}\frac{\partial^2 \theta_1}{\partial y^2} + \lambda \frac{\partial \theta_1}{\partial y} + \left(\frac{\partial U_1}{\partial y}\right)\left(\frac{\partial \overline{U_1}}{\partial y}\right) + \\ + M^2\left\{\frac{1}{1+m^2}\left(U_1 \overline{U_1}\right) + \left(1 - \frac{1}{1+m^2}\right)\frac{s^2}{M^4}\frac{1}{q_{m_1}\overline{q_{m_1}}} + \frac{is}{M^2}\frac{m}{1+m^2}\left(\frac{\overline{U_1}}{q_{m_1}} - \frac{U_1}{\overline{q_{m_1}}}\right)\right\}, \tag{3.22}$$

$$\theta_1(y,t) = g_{13} + g_{14}e^{-\lambda y} - \left(d_{36}e^{d_{23}y} + d_{37}e^{d_{24}y} + d_{38}e^{d_{25}y} + d_{39}e^{d_{26}y} + d_{232}e^{f_{30}y} + \right. \\ \left. + d_{233}e^{f_{31}y} + d_{234}e^{\overline{f_{30}}y} + d_{235}e^{\overline{f_{31}}y} + d_{236}y\right) + \varepsilon\cos\omega t\left(g_{17}e^{g_9 y} + g_{18}e^{g_{10}y} + d_{289}e^{d_{138}y} + \right. \\ \left. + d_{290}e^{d_{139}y} + d_{291}e^{d_{140}y} + d_{292}e^{d_{141}y} + d_{293}e^{\overline{f_{34}}y} + d_{294}e^{\overline{f_{35}}y} + d_{295}e^{f_{34}y} + d_{296}e^{f_{35}y}\right). \tag{3.23}$$

Evaluation of heat transfer coefficient (upper boundary) at $y = 1$ when $Nu_1 = -\left(\frac{d\theta_1}{dy}\right)$

$$Nu_1 = -\Big[-\lambda g_{14}e^{-\lambda} - \Big(d_{36}d_{23}e^{d_{23}} + d_{37}d_{24}e^{d_{24}} + d_{38}d_{25}e^{d_{25}} + d_{39}d_{26}e^{d_{26}} + d_{232}f_{30}e^{f_{30}} + \\ + d_{233}f_{31}e^{f_{31}} + d_{234}\overline{f_{30}}e^{\overline{f_{30}}} + d_{235}\overline{f_{31}}e^{\overline{f_{31}}} + d_{236}\Big) + \varepsilon\cos\omega t\Big(g_{17}g_9e^{g_9} + g_{18}g_{10}e^{g_{10}} + \\ + d_{289}d_{138}e^{d_{138}} + d_{290}d_{139}e^{d_{139}} + d_{291}d_{140}e^{d_{140}} + d_{292}d_{141}e^{d_{141}} + d_{293}\overline{f_{34}}e^{\overline{f_{34}}} + \\ + d_{294}\overline{f_{35}}e^{\overline{f_{35}}} + d_{295}f_{34}e^{f_{34}} + d_{296}f_{35}e^{f_{35}}\Big)\Big]. \tag{3.24}$$

Region-II

$$\frac{\partial\theta_2}{\partial t} = \frac{1}{p_r}\frac{\partial^2\theta_2}{\partial y^2} + (h\rho\alpha\lambda)\frac{\partial\theta_2}{\partial y} + \frac{\beta}{\alpha}\left[\frac{\partial U_2}{\partial y}\right]\left[\frac{\partial \overline{U_2}}{\partial y}\right] + \\ + M^2h^2\beta\left\{\frac{\sigma_1}{1+m^2}\left(U_2\overline{U_2}\right) + \left(1-\frac{\sigma_1}{1+m^2}\right)\frac{s^2}{M^4}\frac{1}{q_{m_2}\overline{q_{m_2}}} + \frac{is}{M^2}\frac{\sigma_2 m}{1+m^2}\left(\frac{\overline{U_2}}{q_{m_2}} - \frac{U_2}{\overline{q_{m_2}}}\right)\right\}, \tag{3.25}$$

$$\theta_2(y,t) = g_{15} + g_{16}e^{-d_{45}y} - \Big(d_{86}e^{d_{74}y} + d_{87}e^{d_{75}y} + d_{88}e^{d_{76}y} + d_{89}e^{d_{77}y} + d_{251}e^{f_{32}y} + \\ + d_{252}e^{f_{33}y} + d_{253}e^{\overline{f_{32}}y} + d_{254}e^{\overline{f_{33}}y} + d_{255}y\Big) + \varepsilon\cos\omega t\Big(g_{19}e^{g_{11}y} + g_{20}e^{g_{12}y} + d_{315}e^{d_{185}y} + \\ + d_{316}e^{d_{186}y} + d_{317}e^{d_{187}y} + d_{318}e^{d_{188}y} + d_{319}e^{\overline{f_{36}}y} + d_{320}e^{\overline{f_{37}}y} + d_{321}e^{f_{36}y} + d_{322}e^{f_{37}y}\Big). \tag{3.26}$$

Evaluation of heat transfer coefficient (lower boundary) at $y = -1$ when $Nu_2 = \dfrac{1}{\beta h}\left(\dfrac{d\theta_2}{dy}\right)$

$$Nu_2 = \frac{1}{\beta h}\Big[-g_{16}d_{45}e^{d_{45}} - \Big(d_{86}d_{74}e^{-d_{74}} + d_{87}d_{75}e^{-d_{75}} + d_{88}d_{76}e^{-d_{76}} + d_{89}d_{77}e^{-d_{77}} + \\ + d_{251}f_{32}e^{-f_{32}} + d_{252}f_{33}e^{-f_{33}} + d_{253}\overline{f_{32}}e^{-\overline{f_{32}}} + d_{254}\overline{f_{33}}e^{-\overline{f_{33}}} - d_{255}\Big) + \\ + \varepsilon\cos\omega t\Big(g_{19}g_{11}e^{-g_{11}} + g_{20}g_{12}e^{-g_{12}} + d_{315}d_{185}e^{-d_{185}} + d_{316}d_{186}e^{-d_{186}} + \\ + d_{317}d_{187}e^{-d_{187}} + d_{318}d_{188}e^{-d_{188}} + d_{319}\overline{f_{36}}e^{-\overline{f_{36}}} + \\ + d_{320}\overline{f_{37}}e^{-\overline{f_{37}}} + d_{321}f_{36}e^{-f_{36}} + d_{322}f_{37}e^{-f_{37}}\Big)\Big]. \tag{3.27}$$

4. Results and discussion

The problem considers the transient MHD flow of an ionized fluid in a horizontal duct formed by two parallel porous surfaces, influenced by a perpendicular magnetic field and modified by Hall current effects. Flow dynamics and current transport equations density are formulated and modified based on the assumptions considered. The resulting differential equations are analytically formulated to determine explicit expressions for both primary, secondary velocity components (u_1, u_2 and w_1, w_2), as well as temperature distributions (θ_1, θ_2) and thermal transfer intensities at the upper and lower boundaries $(Nu_1$ and $Nu_2)$ in both fluid regions.

Approximate analytical solutions for the flow and temperature distribution are derived for electrically conducting fluids. Numerical values for different categories of the key characteristic parameters are computed to analyze their effects on the flow characteristics, and these results are presented through graphical illustrations in Figures 1 to 48. In these figures, continuous lines represent the velocity profiles for transient flow, while mixed dashed and dotted indicators depict the profiles for steady-state conditions.

The figures clearly demonstrate the influence of several parameters: such as the Hartmann number-M, Hall parameter-m, porous parameter-λ, density ratio-ρ, viscosity ratio-α, height ratio-h, electrical conductivity ratio-σ_0 and thermal conductivity-β on the heat exchange processes and fluid dynamic profiles. The study considers two specific cases: $s=0$ and $s=1/2$, representing different ratios fraction of total pressure attributed to electrons.

For the numerical simulations, appropriate quantities for parameters like $(\sigma_{01}=1.2, \sigma_{02}=1.5, P_{r_1}=P_{r_2}=1)$ are employed. Importantly, it is identified that unlike in the case of non-conductive boundaries, the solutions obtained here are influenced by the parameter 's' when the plates possess conducting properties. Furthermore, the findings align well with the results reported by Temburu and Valli [74] for steady-state conditions and are consistent with the earlier work of Malashetty and Leela [55] in scenarios excluding Hall effects and non-porous boundaries under steady flows.

For the case when the ionization parameter, $s = 0$:

Figures 1-3 present how variations in the Hartmann number-M influence the profile of velocity and temperature. Increasing the M weakens the primary and secondary motion in each fluid region, with the highest velocity shifting toward region-I. Likewise, the temperature diminishes with higher values of M, and its maximum also moves toward region-I when other conditions remain unchanged. This may due to the fact that when the magnetic field becomes stronger, the Lorentz force pushes back against the fluid motion, slowing it down. This reduction in flow speed also lowers the temperature, with both velocity and temperature peaks moving toward region I. Although a magnetic field can generate Joule heating, in this case the damping effect on motion dominates.

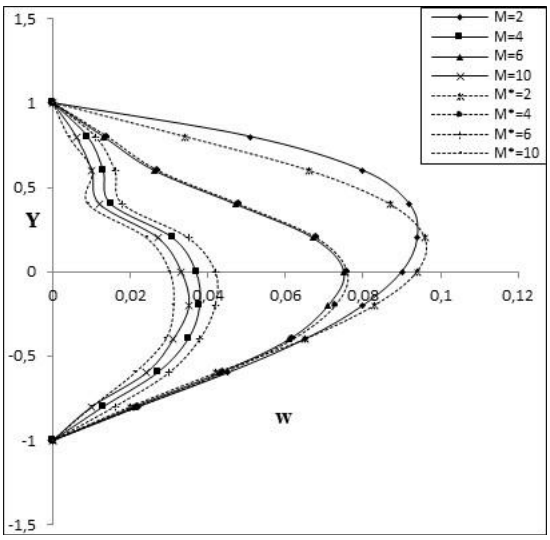

Fig.1. Effect of Hartmann number M on primary velocity components (u_1, u_2) for unsteady and (u_1*, u_2*) steady flow conditions, with fixed values $m=2, \alpha=0.9, \lambda=2, h=1,$ $\sigma_0=1$, $\sigma_{01}=1.2, \sigma_{02}=1.5, \varepsilon=0.5, \rho=1,$ $\omega=1, t=\pi/\omega$ and $s=0$

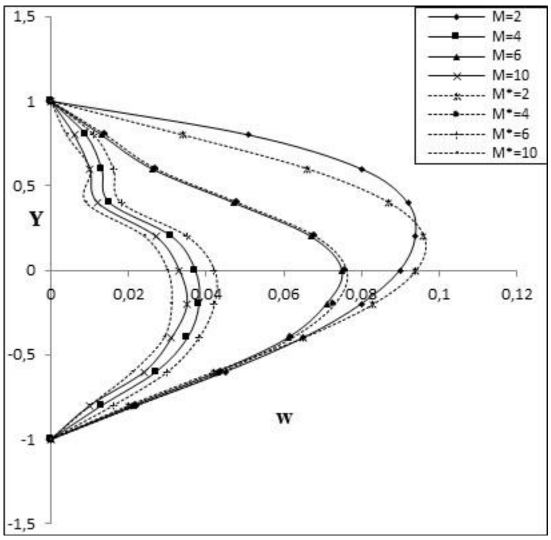

Fig.2. Effect of Hartmann number M on secondary velocity components (w_1, w_2) for unsteady and (w_1*, w_2*) steady flow conditions, with fixed values $m=2, \alpha=0.9, \lambda=2, h=1,$ $\sigma_0=1$, $\sigma_{01}=1.2, \sigma_{02}=1.5, \varepsilon=0.5, \rho=1,$ $\omega=1, t=\pi/\omega$ and $s=0$

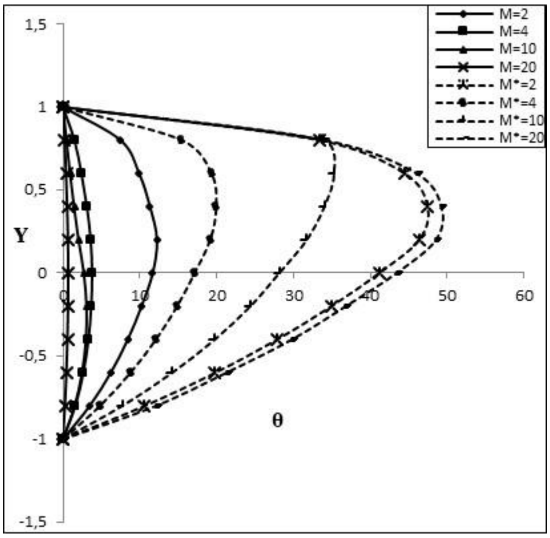

Fig.3. Effect of Hartmann number M on temperature components (θ_1, θ_2) for unsteady and (θ_1^*, θ_2^*) steady flow conditions, with fixed values $m = 2$, $\alpha = 0.333$, $\lambda = 2$, $h = 0.75$, $\sigma_0 = 2$, $\sigma_{01} = 1.2$, $\sigma_{02} = 1.5$, $\beta = 1$, $\varepsilon = 0.5$, $\rho = 1$, $\omega = 1$, $t = \pi / \omega$ and $s = 0$.

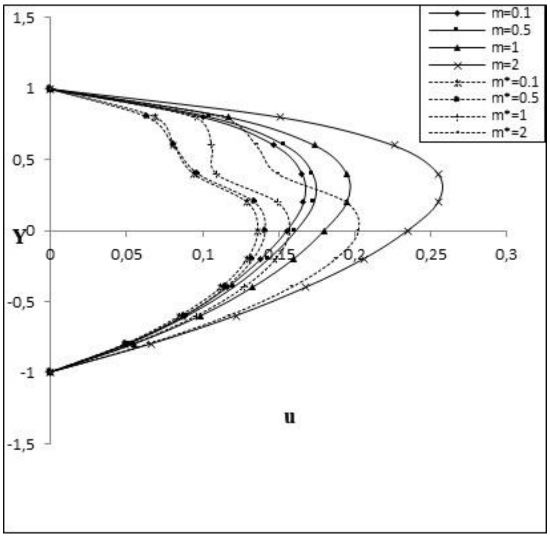

Fig.4. Effect of Hall parameter m on primary velocity components (u_1, u_2) for unsteady and (u_1^*, u_2^*) steady flow conditions, with fixed values $M = 2$, $\alpha = 0.9$, $\lambda = 2$, $h = 1$, $\sigma_0 = 1$, $\sigma_{01} = 1.2$, $\sigma_{02} = 1.5$, $\varepsilon = 0.5$, $\rho = 1$, $\omega = 1$, $t = \pi / \omega$ and $s = 0$

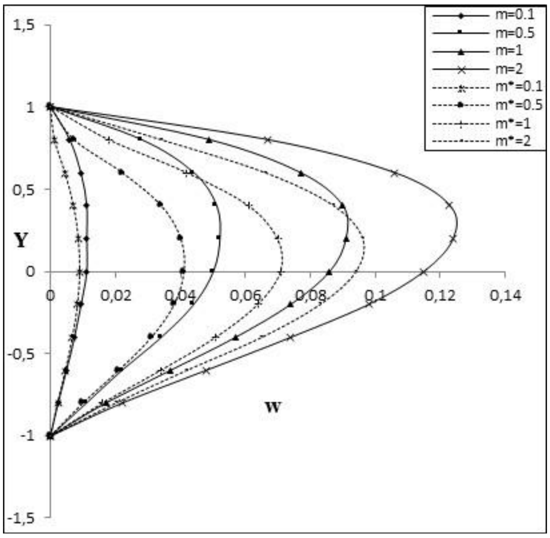

Fig.5. Effect of Hartmann number m on secondary velocity components (w_1, w_2) for unsteady and (w_1^*, w_2^*) steady flow conditions, with fixed values $M = 2$, $\alpha = 0.9$, $\lambda = 2$, $h = 1$, $\sigma_0 = 1$, $\sigma_{01} = 1.2$, $\sigma_{02} = 1.5$, $\varepsilon = 0.5$, $\rho = 1$, $\omega = 1$, $t = \pi / \omega$ and $s = 0$.

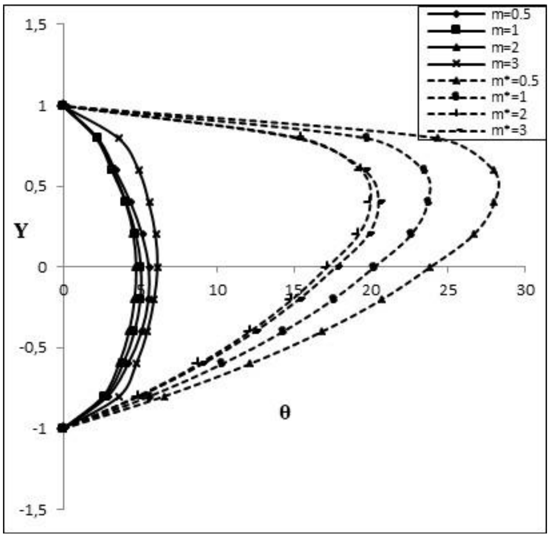

Fig.6. Effect of Hartmann number m on temperature components (θ_1, θ_2) for unsteady and (θ_1^*, θ_2^*) steady flow conditions, with fixed values $M = 2$, $\alpha = 0.333$, $\lambda = 2$, $h = 0.75$, $\sigma_0 = 2$, $\sigma_{01} = 1.2$, $\sigma_{02} = 1.5$, $\beta = 1$, $\varepsilon = 0.5$, $\rho = 1$, $\omega = 1$, $t = \pi / \omega$ and $s = 0$.

Figures 4-6 illustrate how variations in the Hall parameter-influence the velocity and temperature profiles. With a rise in the value of m, both dominant and transverse velocity profiles exhibit growth, with their respective peaks migrating toward region-I. The temperature reduces up to $m = 2$, after which it rises, while the location of the maximum temperature shifts toward region-I similarly. That is, as the Hall parameter increases, the Hall current changes the way the magnetic field interacts with the moving fluid. This weakens the braking effect of the Lorentz force, allowing velocities to rise and shifting their peaks toward region I. The temperature first drops up to about $m = 2$ because stronger mixing removes heat more efficiently, but after that it starts to climb again due to reduced cooling efficiency.

The contribution of the porous parameter-λ to changes in velocity and temperature fields is displayed in Figs 7-9. From Fig.7, it is evident that in region-I, λ promotes higher primary velocity, while in region-II, it causes a decline. Figure 8 reveals that secondary velocity increases in region-I up to $\lambda = 1.5$ and then declines, while it decreases steadily in region-II. Both velocity profiles tend to shift toward region-I with higher values of λ. Figure 9 indicates that temperature drops up to $\lambda = 1$ in region-I and then begins to rise, whereas in region-II, it continuously decreases, with the temperature peak moving toward region-I as λ increases. That is, changing the porous nature of the channel plates affect how easily fluid can pass through or interact with them. In some regions, greater permeability lets the fluid move more freely, boosting velocities, while in others it increases resistance and slows the flow. This uneven change across the regions shifts where the maximum velocity and temperature occur.

Figures 10-12 illustrate how the viscosity ratio α affects velocity and temperature. Increasing α results in higher primary and secondary velocities, with the peak values drifting toward region-I. Temperature declines up to $\alpha = 0.1$ in region-I and $\alpha = 0.333$ in region-II before increasing. The highest temperature gradually shifts below the centerline of the channel toward Region-II as α enhances.

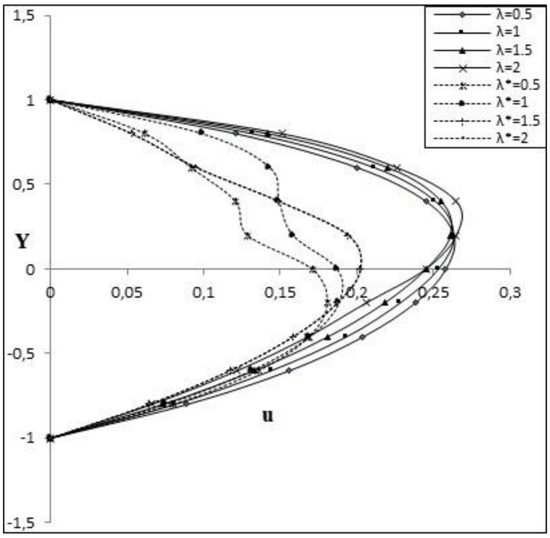

Fig.7. Effect of porous parameter λ on primary velocity components (u_1, u_2) for unsteady and $(u_1{*}, u_2{*})$ steady flow conditions, with fixed values $M = 2, \alpha = 0.9, m = 2, h = 1, \sigma_0 = 1, \sigma_{01} = 1.2, \sigma_{02} = 1.5, \varepsilon = 0.5, \rho = 1, \omega = 1, t = \pi / \omega$ and $s = 0$.

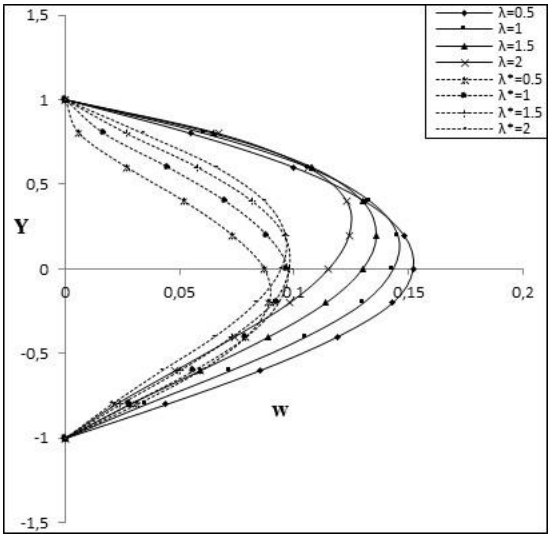

Fig.8. Effect of porous parameter λ on primary velocity components (w_1, w_2) for unsteady and $(w_1{*}, w_2{*})$ steady flow conditions, with fixed values $M = 2, \alpha = 0.9, m = 2, h = 1, \sigma_0 = 1, \sigma_{01} = 1.2, \sigma_{02} = 1.5, \varepsilon = 0.5, \rho = 1, \omega = 1, t = \pi / \omega$ and $s = 0$.

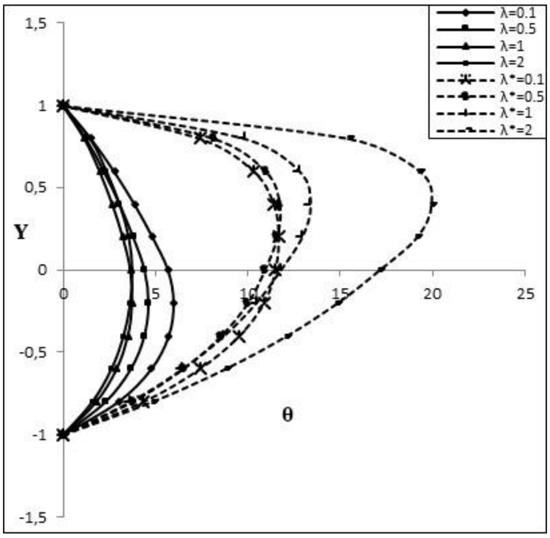

Fig.9. Effect of porous parameter λ on temperature components (θ_1, θ_2) for unsteady and $(\theta_1{}^*, \theta_2{}^*)$ steady flow conditions, with fixed values $M = 4$, $\alpha = 0.333$, $m = 2$, $h = 0.75$, $\sigma_0 = 2$, $\sigma_{01} = 1.2$, $\sigma_{02} = 1.5$, $\beta = 1$, $\varepsilon = 0.5$, $\rho = 1$, $\omega = 1$, $t = \pi / \omega$ and $s = 0$.

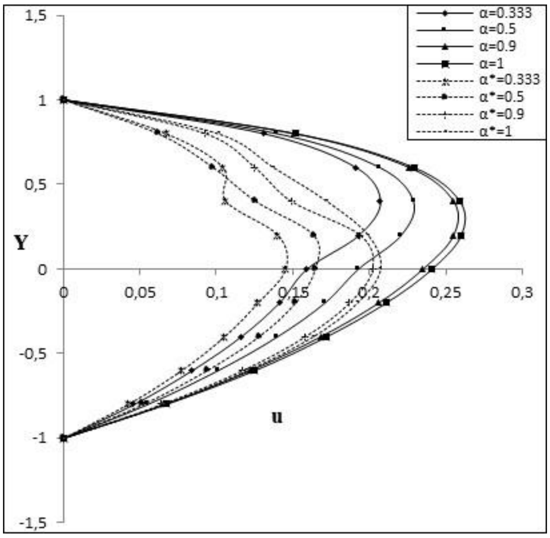

Fig.10. Effect of viscosity ratio α on primary velocity components (u_1, u_2) for unsteady and $(u_1{}^*, u_2{}^*)$ steady flow conditions, with fixed values $M = 2, \lambda = 2, m = 2, h = 1$, $\sigma_0 = 1$, $\sigma_{01} = 1.2, \sigma_{02} = 1.5, \varepsilon = 0.5, \rho = 1$, $\omega = 1$, $t = \pi / \omega$ and $s = 0$.

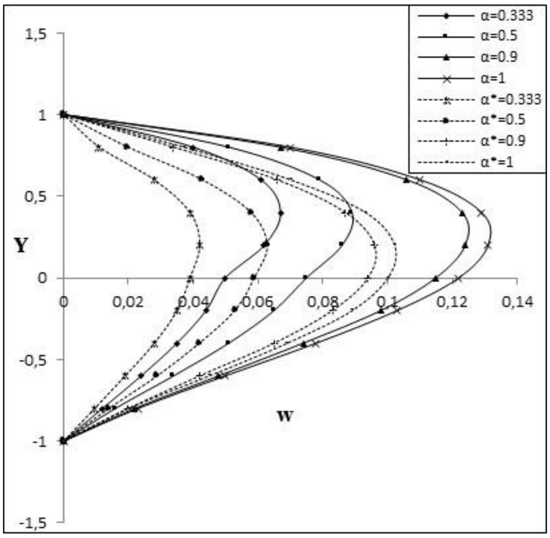

Fig.11. Effect of viscosity ratio α on secondary velocity components (w_1, w_2) for unsteady and $(w_1{}^*, w_2{}^*)$ steady flow conditions, with fixed values $M = 2$, $\lambda = 2$, $m = 2$ $h = 1$, $\sigma_0 = 1$, $\sigma_{01} = 1.2, \sigma_{02} = 1.5, \varepsilon = 0.5$, $\rho = 1$, $\omega = 1$, $t = \pi / \omega$ and $s = 0$.

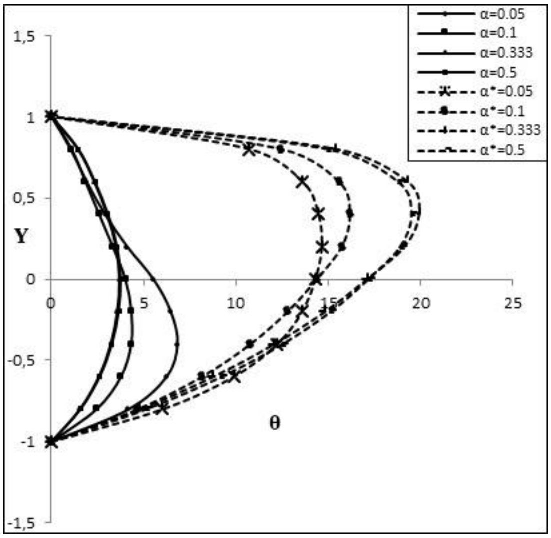

Fig.12. Effect of viscosity ratio α on temperature components (θ_1, θ_2) for unsteady and $(\theta_1{}^*, \theta_2{}^*)$ steady flow conditions, with fixed values $M = 4$, $m = 2$, $\lambda = 2$, $h = 0.75$, $\sigma_0 = 2$, $\sigma_{01} = 1.2$, $\sigma_{02} = 1.5$, $\beta = 1$, $\varepsilon = 0.5$, $\rho = 1$, $\omega = 1$, $t = \pi / \omega$ and $s = 0$.

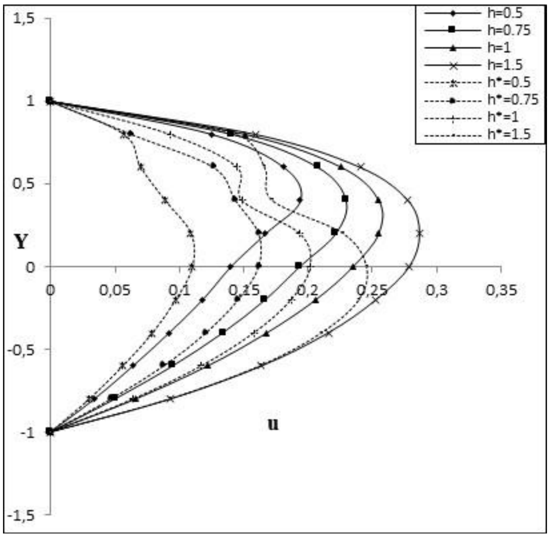

Fig.13. Effect of height ratio *h* on primary velocity components (u_1, u_2) for unsteady and (u_1^*, u_2^*) steady flow conditions, with fixed values $M=2, \alpha=0.9, m=2, \lambda=2,$ $\sigma_0=1$, $\sigma_{01}=1.2, \sigma_{02}=1.5, \varepsilon=0.5, \rho=1,$ $\omega=1$, $t=\pi/\omega$ and $s=0$.

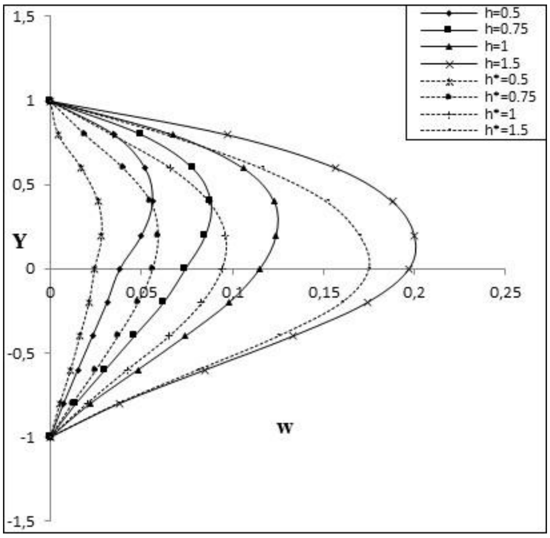

Fig.14. Effect of height ratio *h* on secondary velocity components (w_1, w_2) for unsteady and (w_1^*, w_2^*) steady flow conditions, with fixed values $M=2, \alpha=0.9, m=2, \lambda=2,$ $\sigma_0=1$, $\sigma_{01}=1.2, \sigma_{02}=1.5, \varepsilon=0.5, \rho=1,$ $\omega=1$, $t=\pi/\omega$ and $s=0$.

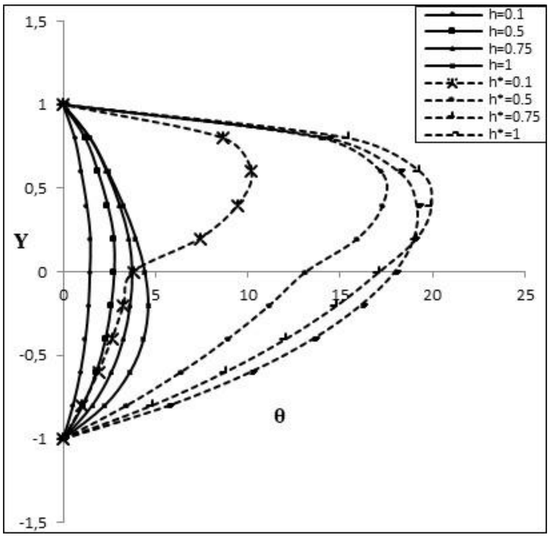

Fig.15. Effect of height ratio *h* on temperature components (θ_1, θ_2) for unsteady and (θ_1^*, θ_2^*) steady flow conditions, with fixed values $M=4$, $m=2$, $\lambda=2$, $\alpha=0.333$, $\sigma_0=2$, $\sigma_{01}=1.2$, $\sigma_{02}=1.5$, $\beta=1$, $\varepsilon=0.5$, $\rho=1$, $\omega=1$, $t=\pi/\omega$ and $s=0$.

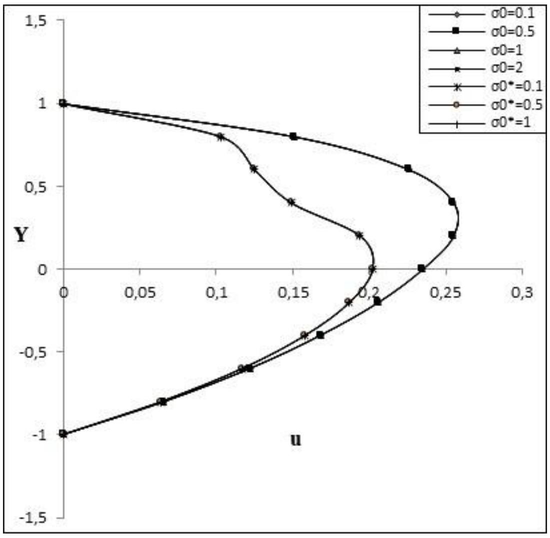

Fig.16. Effect of electrical conductivity ratio σ_0 on primary velocity components (u_1, u_2) for unsteady and (u_1^*, u_2^*) steady flow conditions, with fixed values $M=2, \alpha=0.9, m=2, \lambda=2,$ $\sigma_{01}=1.2,$ $h=1,$ $\sigma_{02}=1.5, \varepsilon=0.5, \rho=1,$ $\omega=1,$ $t=\pi/\omega$ and $s=0$.

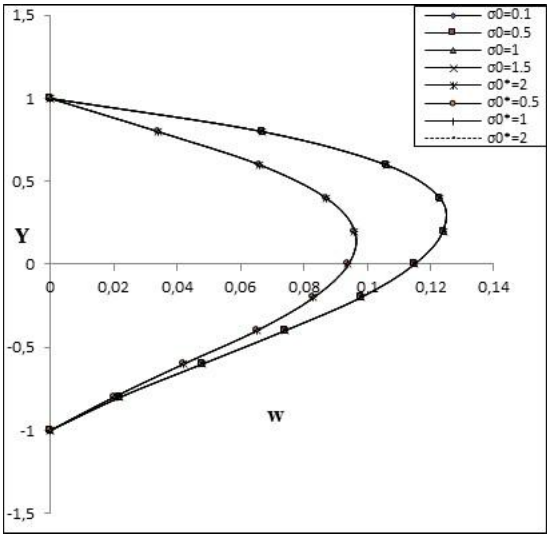

Fig.17. Effect of electrical conductivity ratio σ_0 on secondary velocity components $(w_1,\ w_2)$ for unsteady and $(w_1^*,\ w_2^*)$ steady flow conditions, with fixed values $M=2$, $m=2$, $\lambda=2$, $\alpha=0.9$, $h=1$, $\sigma_{01}=1.2$, $\sigma_{02}=1.5$, $\varepsilon=0.5$, $\rho=1$, $\omega=1$, $t=\pi/\omega$ and $s=0$.

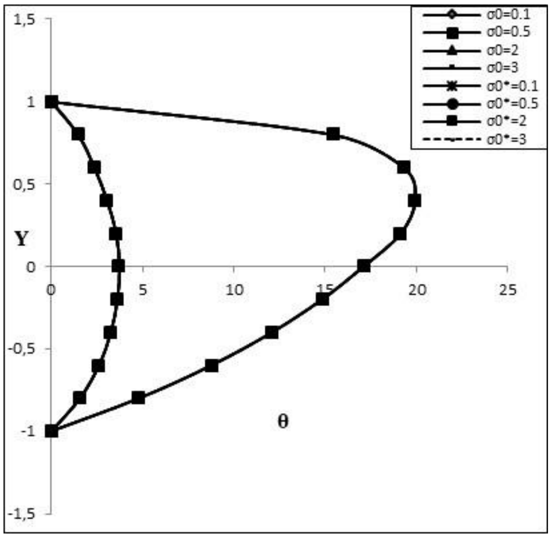

Fig.18. Effect of electrical conductivity ratio σ_0 on temperature components (θ_1,θ_2) for unsteady and (θ_1^*,θ_2^*) steady flow conditions, with fixed values $M=4$, $m=2$, $\lambda=2$, $\alpha=0.333$, $h=0.75$, $\sigma_{01}=1.2$, $\sigma_{02}=1.5$, $\beta=1$, $\varepsilon=0.5$, $\rho=1$, $\omega=1$, $t=\pi/\omega$ and $s=0$.

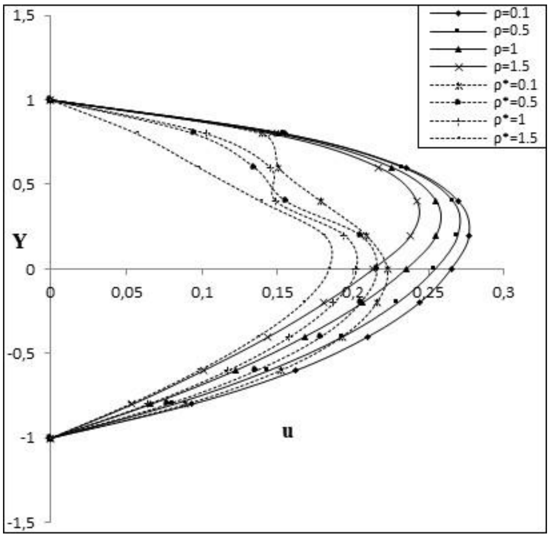

Fig.19. Effect of density ratio ρ on primary velocity components $(u_1,\ u_2)$ for unsteady and $(u_1^*,\ u_2^*)$ steady flow conditions, with fixed values $M=2, \alpha=0.9, m=2, \lambda=2,$ $\sigma_0=1$, $\sigma_{01}=1.2, \sigma_{02}=1.5, \varepsilon=0.5, h=1,$ $\omega=1$, $t=\pi/\omega$ and $s=0$.

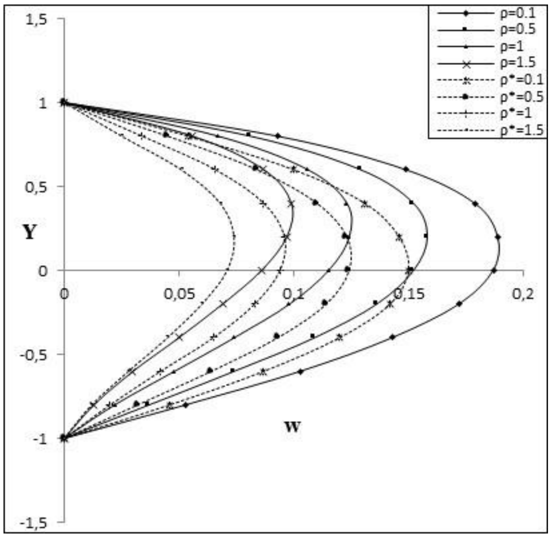

Fig.20. Effect of density ratio ρ on secondary velocity components $(w_1,\ w_2)$ for unsteady and $(w_1^*,\ w_2^*)$ steady flow conditions, with fixed values $M=2, \alpha=0.1, m=2, \lambda=2,$ $\sigma_0=2$, $\sigma_{01}=1.2, \sigma_{02}=1.5, \varepsilon=0.5, h=1,$ $\omega=1$, $t=\pi/\omega$ and $s=0$.

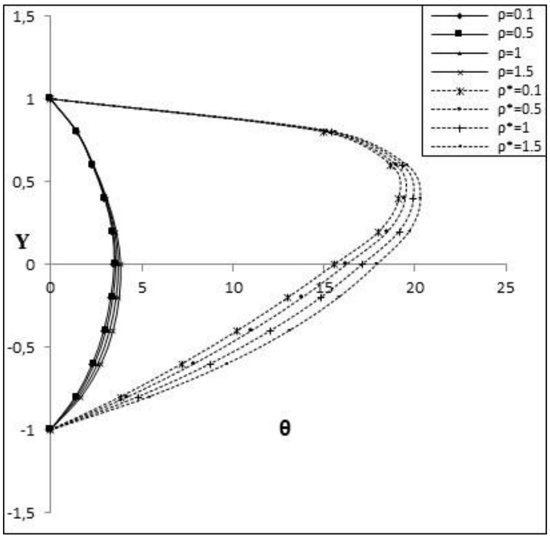

Fig.21. Effect of density ratio ρ on temperature components (θ_1,θ_2) for unsteady and $(\theta_1{*},\theta_2{*})$ steady flow conditions, with fixed values $M=4$, $m=2$, $\lambda=2$, $\alpha=0.333$, $h=0.75$, $\sigma_0=2$, $\sigma_{01}=1.2$, $\sigma_{02}=1.5$, $\varepsilon=0.5$, $\beta=1$, $\omega=1$, $t=\pi/\omega$ and $s=0$.

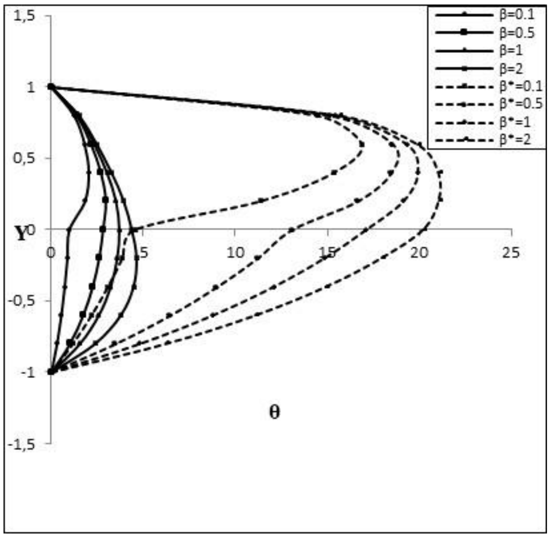

Fig.22. Effect of thermal conductivity ratio β on temperature components (θ_1,θ_2) for unsteady and $(\theta_1{*},\theta_2{*})$ steady flow conditions, with fixed values $M=4$, $m=2$, $\lambda=2$, $\alpha=0.333$, $h=0.75$, $\sigma_0=2$, $\sigma_{01}=1.2$, $\sigma_{02}=1.5$, $\varepsilon=0.5$, $\rho=1$, $\omega=1$, $t=\pi/\omega$ and $s=0$.

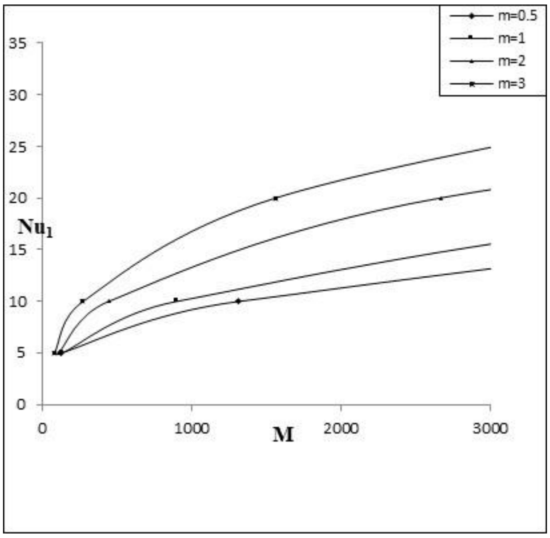

Fig.23. Variation of Nusselt number Nu_1 with different Hartmann number M values for fixed parameters $\alpha=0.333$, $\sigma_0=2$, $\lambda=1$, $\sigma_{01}=1.2$, $\sigma_{02}=1.5$, $\rho=1$, $h=0.75$, $\beta=1$, $\varepsilon=0.5$, $\omega=1$, $t=\pi/\omega$ and $s=0$.

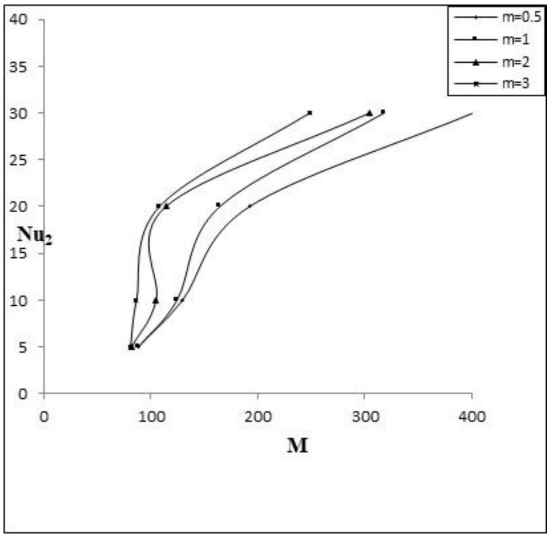

Fig.24. Variation of Nusselt number Nu_2 with different Hartmann number M values for fixed parameters $\alpha=0.333$, $\sigma_0=2$, $\lambda=1$, $\sigma_{01}=1.2$, $\sigma_{02}=1.5$, $\rho=1$, $h=0.75$, $\beta=1$, $\varepsilon=0.5$, $\omega=1$, $t=\pi/\omega$ and $s=0$.

Figures 13-15 illustrate how the flow and heat transfer characteristics respond to different values of the height ratio-*h*. Increasing *h* results in improved magnitudes of both primary and secondary fluid motions, with the peaks approaching region-I. Temperature distribution also rises throughout both regions, while the location of the maximum temperature moves downward from the channel midpoint into region-II as *h* rises.

Figures 16-18 show how the electrical conductivity ratio impacts the system-σ_0. Changes in σ_0 do not significantly alter the velocity or temperature values, but the peak positions shift toward region-I above the channel centerline with increasing σ_0.

Figures 19-21 explore how variations in ρ influence the flow and thermal distributions. As ρ increases, both primary and secondary velocities diminish, moving toward region-I. The temperature rises in both regions, with the peak shifting below the channel centerline into region-II.

Figures 16-18 show how the electrical conductivity ratio impacts the system-σ_0. Changes in σ_0 do not significantly alter the velocity or temperature values, but the peak positions shift toward region-I above the channel centerline with increasing σ_0.

Figures 19-21 explore how variations in ρ influence the flow and thermal distributions. As ρ increases, both primary and secondary velocities diminish, moving toward region-I. The temperature rises in both regions, with the peak shifting below the channel centerline into region-II.

Figure 22 illustrates the influence of thermal conductivity ratio-β variations on the temperature profile. As β increases, temperature levels rise in both regions, with the peak slightly moving downward from the channel centerline into region-II. That is, better thermal conductivity smooth's out temperature differences by spreading heat more evenly.

The heat exchange rates at both the upper and lower channel interfaces are represented in Figs 23 and 24. As the Hartmann number-M rises, heat flow rate improves when $s = 0$, while other parameters are kept constant. Additionally, a rise in the Hall parameter contributes to greater heat dissipation at the channel surfaces.

That is, both a stronger magnetic field and a higher Hall parameter increase the overall heat transfer by modifying how the fluid moves and how electrical energy is converted into heat.

For the case when the ionization parameter, *s = 1/2*:

Figures 25-27 display how the Hartmann number-*M* affects flow dynamics and heat transfer behavior. With increasing *M*, an increase in *M* up to 4 leads to a reduction in the primary velocity, accompanied by a corresponding initial increase in the secondary velocity exhibits a rising trend initially and later declines in both regions. The location of peak velocity gradually ascends beyond the centerline toward region-I. Simultaneously, the temperature variation declines as *M* increases, and the maximum temperature shifts toward region-I when other conditions remain unchanged. This means that, a stronger magnetic field slows the primary flow because the Lorentz force resists motion. The secondary velocity responds differently, first rising due to altered cross-flow currents, then falling as magnetic damping dominates. In both cases, the temperature decreases, and the main peaks shift toward region I.

Figures 28-30 illustrate the effect of Hall parameter-*m* on flow velocity and temperature distribution. An increase in *m* results in the enhancement of both primary and secondary velocities. The peak primary velocity moves toward region-I, while the peak secondary velocity drifts toward region-II. Elevated Hall parameter values lead to reduced temperatures in both regions and a downward shift of the thermal maximum into region-II. That is, the increasing the Hall parameter boosts both primary and secondary velocities. The change in current direction from Hall effects moves the primary velocity peak into region I, while the secondary velocity peak shifts into region II. Temperature drops steadily, with its maxima also shifting toward region II, indicating that heat transport is more pronounced there.

Figures 31-33 represent how changing the porous parameter-λ affects both the flow and temperature characteristics within the two-fluid system. As λ rises, the main flow speed increases in region-I, but reduces in region-II. Secondary flow component grows until it reaches a peak at $\lambda = 1$, then declines in region-I and keeps decreasing in region-II.

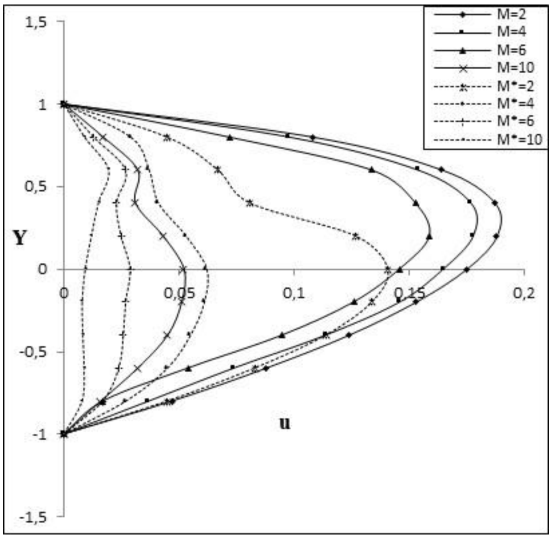

Fig.25. Effect of Hartmann number M on primary velocity components (u_1, u_2) for unsteady and (u_1^*, u_2^*) steady flow conditions, with fixed values $m=2$, $\alpha=0.9$, $\lambda=2$, $h=1$, $\sigma_0=1$, $\sigma_{01}=1.2$, $\sigma_{02}=1.5$, $\varepsilon=0.5$, $\rho=1$, $\omega=1$, $t=\pi/\omega$ and $s=0.5$.

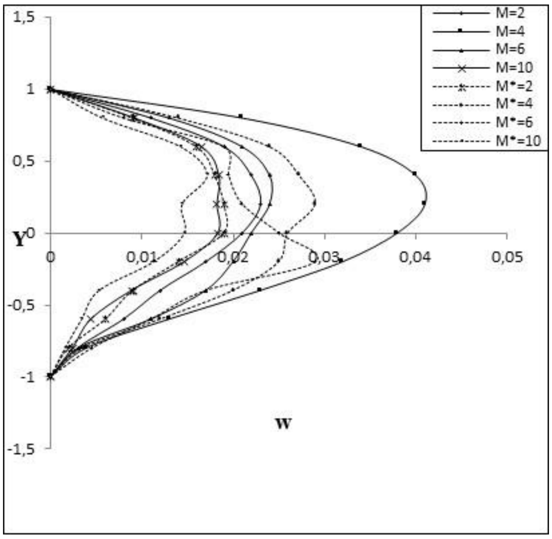

Fig.26. Effect of Hartmann number M on secondary velocity components (w_1, w_2) for unsteady and (w_1^*, w_2^*) steady flow conditions, with fixed values $m=2$, $\alpha=0.9$, $\lambda=2$, $h=1$, $\sigma_0=1$, $\sigma_{01}=1.2$, $\sigma_{02}=1.5$, $\varepsilon=0.5$, $\rho=1$, $\omega=1$, $t=\pi/\omega$ and $s=0.5$.

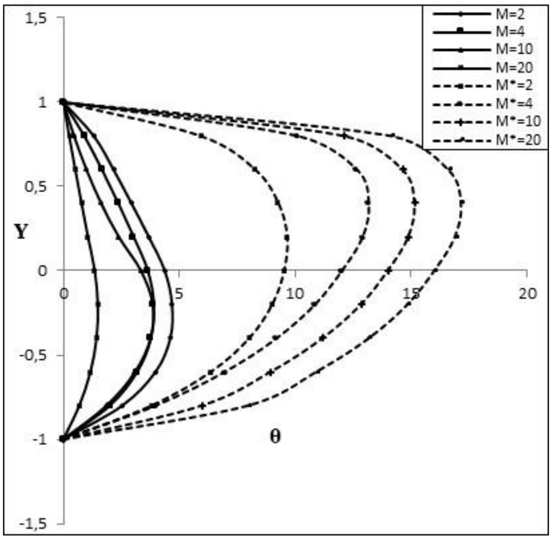

Fig.27. Effect of Hartmann number M on temperature components (θ_1, θ_2) for unsteady and (θ_1^*, θ_2^*) steady flow conditions, with fixed values $m=2$, $\alpha=0.333$, $\lambda=2$, $h=0.75$, $\sigma_0=2$, $\sigma_{01}=1.2$, $\sigma_{02}=1.5$, $\beta=1$, $\varepsilon=0.5$, $\rho=1$, $\omega=1$, $t=\pi/\omega$ and $s=0.5$.

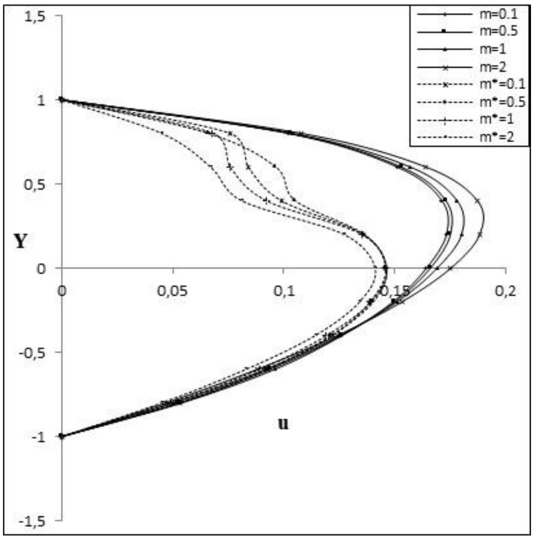

Fig.28. Effect of Hall parameter m on primary velocity components (u_1, u_2) for unsteady and (u_1^*, u_2^*) steady flow conditions, with fixed values $M=2$, $\alpha=0.9$, $\lambda=2$, $h=1$, $\sigma_0=1$, $\sigma_{01}=1.2$, $\sigma_{02}=1.5$, $\varepsilon=0.5$, $\rho=1$, $\omega=1$, $t=\pi/\omega$ and $s=0.5$.

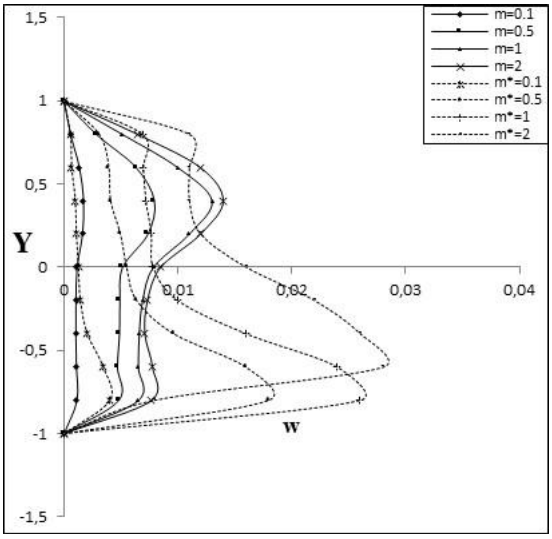

Fig.29. Effect of Hartmann number m on secondary velocity components $\left(w_1,\ w_2\right)$ for unsteady and $\left(w_1{}^*,\ w_2{}^*\right)$ steady flow conditions, with fixed values $M=2, \alpha=0.9, \lambda=2, h=1, \sigma_0=1, \quad \sigma_{01}=1.2, \sigma_{02}=1.5, \varepsilon=0.5, \rho=1, \omega=1, t=\pi/\omega$ and $s=0.5$.

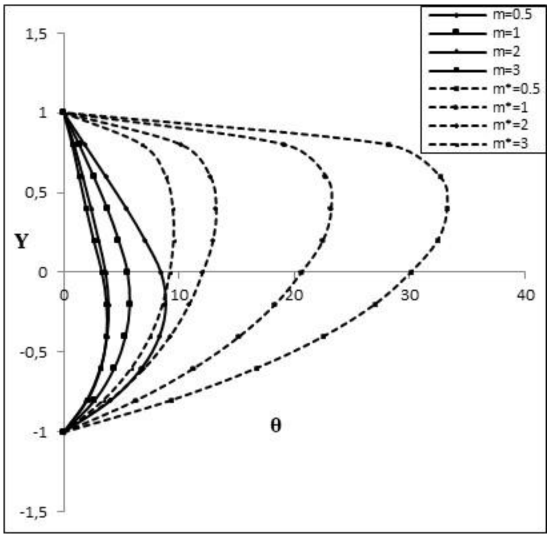

Fig.30. Effect of Hartmann number m on temperature components $\left(\theta_1,\theta_2\right)$ for unsteady and $\left(\theta_1{}^*,\theta_2{}^*\right)$ steady flow conditions, with fixed values $M=2,\ \alpha=0.333,\ \lambda=2,\ h=0.75,\ \sigma_0=2,\ \sigma_{01}=1.2,\ \sigma_{02}=1.5,\ \beta=1,\ \varepsilon=0.5,\ \rho=1,\ \omega=1,\ t=\pi/\omega$ and $s=0.5$.

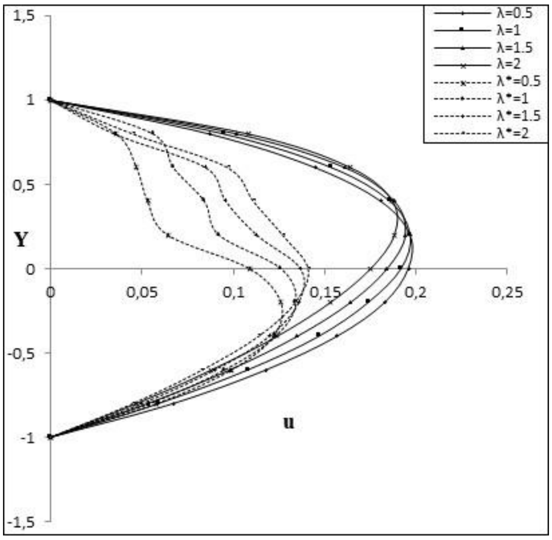

Fig.31. Effect of porous parameter λ on primary velocity components $\left(u_1,\ u_2\right)$ for unsteady and $\left(u_1{}^*,\ u_2{}^*\right)$ steady flow conditions, with fixed values $M=2, \alpha=0.9, m=2, h=1, \sigma_0=1, \quad \sigma_{01}=1.2, \sigma_{02}=1.5, \varepsilon=0.5, \rho=1, \omega=1, t=\pi/\omega$ and $s=0.5$.

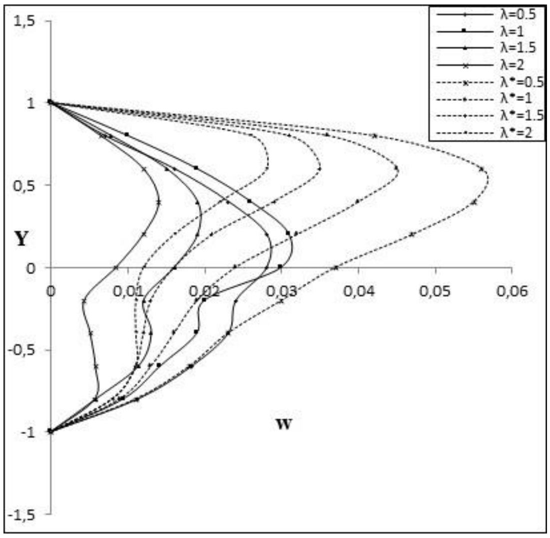

Fig.32. Effect of porous parameter λ on primary velocity components $\left(w_1,\ w_2\right)$ for unsteady and $\left(w_1{}^*,\ w_2{}^*\right)$ steady flow conditions, with fixed values $M=2, \alpha=0.9, m=2, h=1, \sigma_0=1, \quad \sigma_{01}=1.2, \sigma_{02}=1.5, \varepsilon=0.5, \rho=1, \omega=1, t=\pi/\omega$ and $s=0.5$.

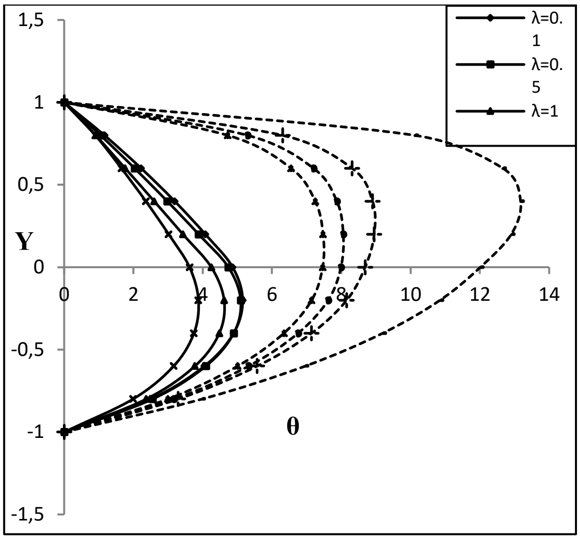

Fig.33. Effect of porous parameter λ on temperature components (θ_1, θ_2) for unsteady and (θ_1^*, θ_2^*) steady flow conditions, with fixed values $M = 4$, $\alpha = 0.333$, $m = 2$, $h = 0.75$, $\sigma_0 = 2$, $\sigma_{01} = 1.2$, $\sigma_{02} = 1.5$, $\beta = 1$, $\varepsilon = 0.5$, $\rho = 1$, $\omega = 1$, $t = \pi / \omega$ and $s = 0.5$.

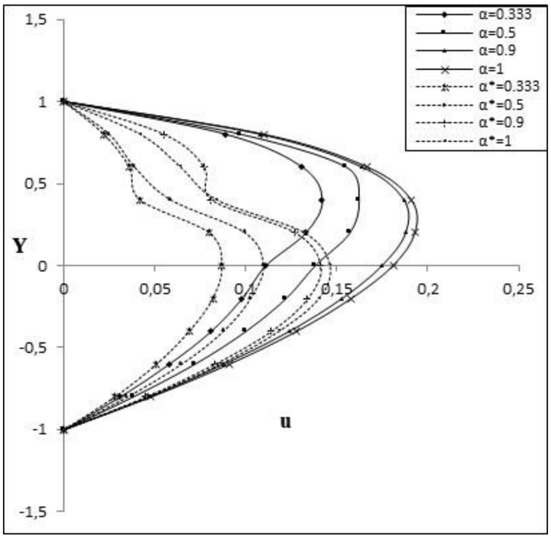

Fig.34. Effect of viscosity ratio α on primary velocity components (u_1, u_2) for unsteady and (u_1^*, u_2^*) steady flow conditions, with fixed values $M = 2, \lambda = 2, m = 2, h = 1$, $\sigma_0 = 1$, $\sigma_{01} = 1.2, \sigma_{02} = 1.5, \varepsilon = 0.5, \rho = 1$, $\omega = 1$, $t = \pi / \omega$ and $s = 0.5$.

The peak velocity location also migrates upward from the mid-plane into region-I. Alongside these changes, the temperature profiles in both flow areas decrease, with the highest temperature point gradually shifting toward region-I as the porous parameter grows.

Figures 34-36 present the viscosity ratio-α on fluid motion and heat distribution. With higher viscosity ratios, the dominant velocity component rises in both regions. The secondary velocity, however, decreases until a certain point $\alpha = 0.5$, then starts rising in region-I, while continuously declining in region-II. The peak velocity shifts upward across the centerline into region-I. The temperature initially drops up to a particular viscosity ratio $\alpha = 0.1$ in region-I as well as $\alpha = 0.333$ in region-II, progressively elevates, with the peak temperature moving beneath the flow's midline in region-II as α grows. That is, wall permeability and viscous diffusion influence the flow differently across the two regions. Depending on whether drag or momentum redistribution dominates, peaks in velocity and temperature shift location, reflecting the competition between wall-induced resistance and fluid mixing.

Figures 37-39 illustrate the impact of height ratio-h variations on flow velocity and temperature fields. With an increase in *h* the primary velocity shows a noticeable increase throughout both fluid layers. In contrast, the secondary velocity decreases up to $h = 0.75$, after which it ascends in region-I and steadily rises in region-II. The zone of maximum flow velocity moves upward from the channel's central axis toward region-I. Likewise, the temperature profiles display a gradual rise in both regions, with the thermal peak shifting downward into region-II as 'h' becomes larger. That is, altering the channel height ratio changes the flow speed distribution by modifying the geometric constraints on momentum diffusion.

Figures 40-42 explore the influence of the electrical conductivity ratio-σ_0 on flow and thermal characteristics. As the conductivity ratio grows, in both regions, the axial (primary) velocity shows an increase, whereas the transverse (secondary) velocity declines in region-I and region-II up to a certain value $\sigma_0 = 1$, and then begins to increase. The peak flow velocity shifts above the midline into region-I.

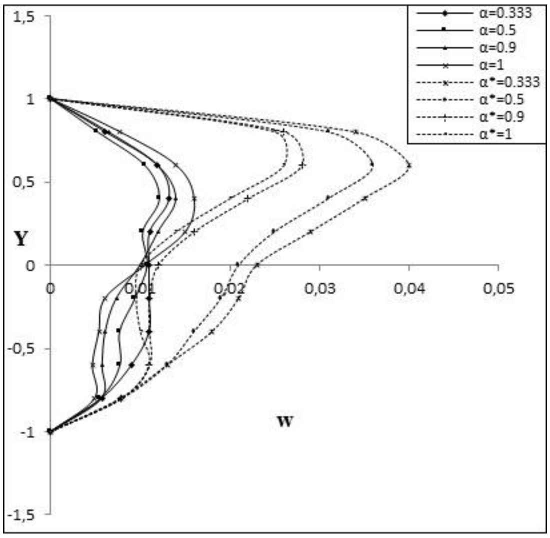

Fig.35. Effect of viscosity ratio α on secondary velocity components (w_1, w_2) for unsteady and $(w_1{*}, w_2{*})$ steady flow conditions, with fixed values $M=2$, $\lambda=2$, $m=2$ $h=1$, $\sigma_0=1$, $\sigma_{01}=1.2$, $\sigma_{02}=1.5$, $\varepsilon=0.5$, $\rho=1$, $\omega=1$, $t=\pi/\omega$ and $s=0.5$.

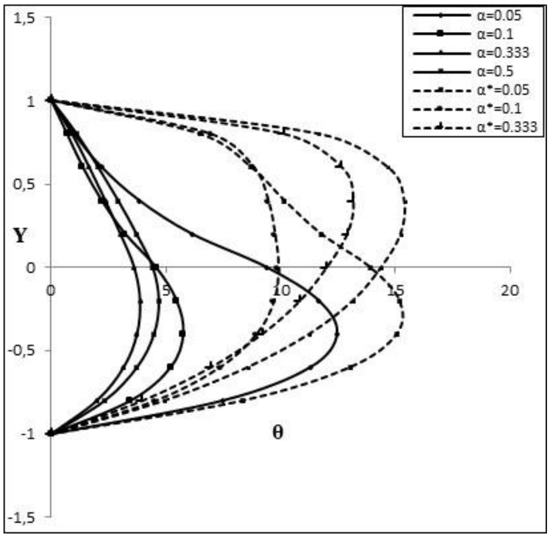

Fig.36. Effect of viscosity ratio α on temperature components (θ_1, θ_2) for unsteady and $(\theta_1{*}, \theta_2{*})$ steady flow conditions, with fixed values $M=4$, $m=2$, $\lambda=2$, $h=0.75$, $\sigma_0=2$, $\sigma_{01}=1.2$, $\sigma_{02}=1.5$, $\beta=1$, $\varepsilon=0.5$, $\rho=1$, $\omega=1$, $t=\pi/\omega$ and $s=0.5$.

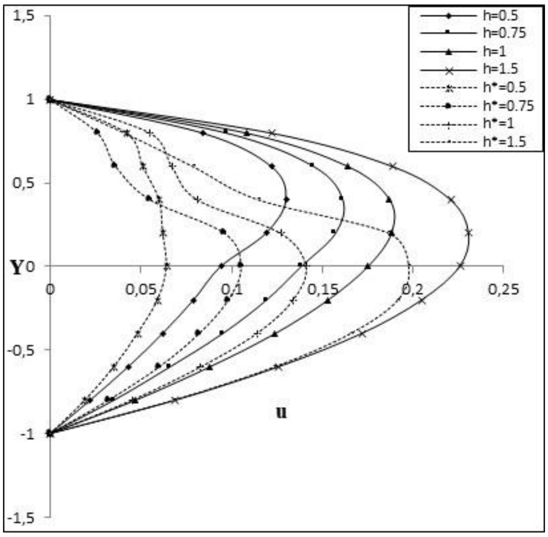

Fig.37. Effect of height ratio h on primary velocity components (u_1, u_2) for unsteady and $(u_1{*}, u_2{*})$ steady flow conditions, with fixed values $M=2$, $\alpha=0.9$, $m=2$, $\lambda=2$, $\sigma_0=1$, $\sigma_{01}=1.2$, $\sigma_{02}=1.5$, $\varepsilon=0.5$, $\rho=1$, $\omega=1$, $t=\pi/\omega$ and $s=0.5$.

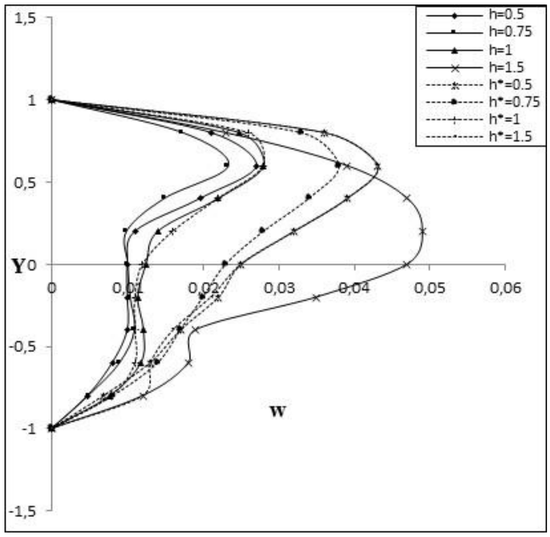

Fig.38. Effect of height ratio h on secondary velocity components (w_1, w_2) for unsteady and $(w_1{*}, w_2{*})$ steady flow conditions, with fixed values $M=2$, $\alpha=0.9$, $m=2$, $\lambda=2$, $\sigma_0=1$, $\sigma_{01}=1.2$, $\sigma_{02}=1.5$, $\varepsilon=0.5$, $\rho=1$, $\omega=1$, $t=\pi/\omega$ and $s=0.5$.

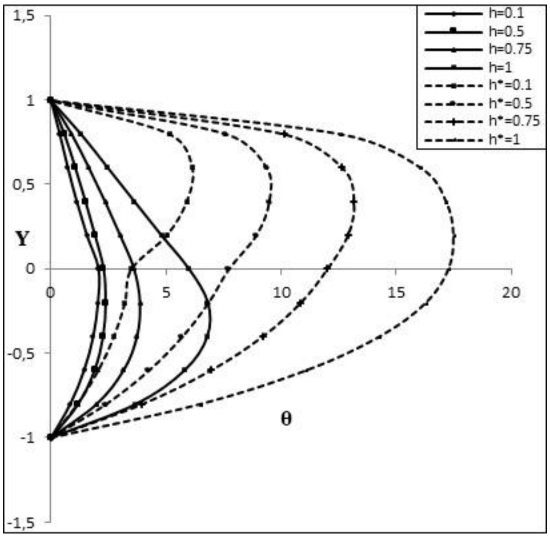

Fig.39. Effect of height ratio h on temperature components (θ_1, θ_2) for unsteady and (θ_1^*, θ_2^*) steady flow conditions, with fixed values $M = 4$, $m = 2$, $\lambda = 2$, $\alpha = 0.333$, $\sigma_0 = 2$, $\sigma_{01} = 1.2$, $\sigma_{02} = 1.5$, $\beta = 1$, $\varepsilon = 0.5$, $\rho = 1$, $\omega = 1$, $t = \pi / \omega$ and $s = 0.5$.

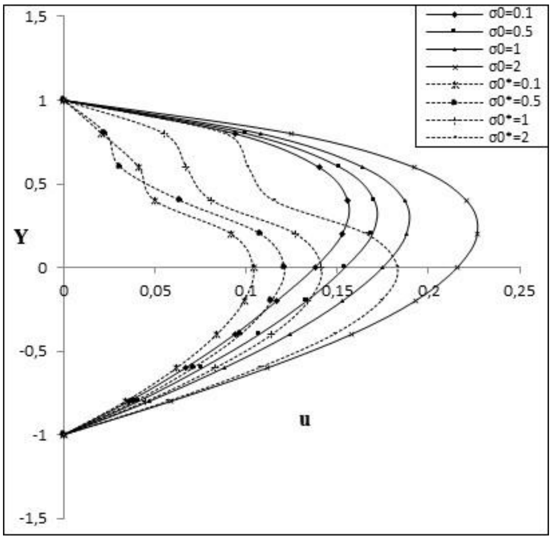

Fig.40. Effect of electrical conductivity ratio σ_0 on primary velocity components (u_1, u_2) for unsteady and (u_1^*, u_2^*) steady flow conditions, with fixed values $M = 2$, $\alpha = 0.9$, $m = 2$, $\lambda = 2$, $\sigma_{01} = 1.2$, $h = 1$, $\rho = 1$, $\sigma_{02} = 1.5$, $\varepsilon = 0.5$, $\omega = 1$, $t = \pi / \omega$ and $s = 0.5$.

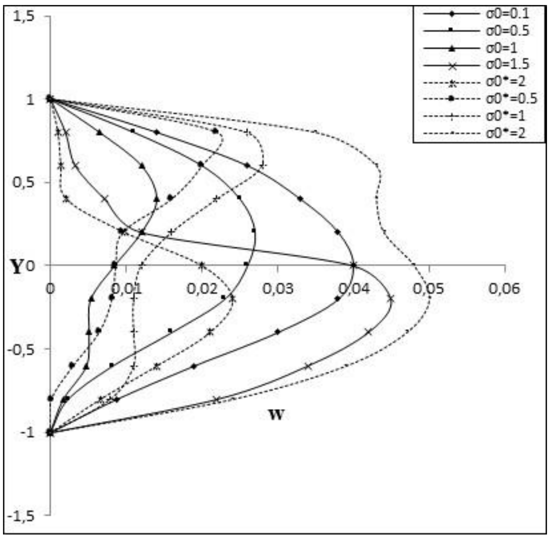

Fig.41. Effect of electrical conductivity ratio σ_0 on secondary velocity components (w_1, w_2) for unsteady and (w_1^*, w_2^*) steady flow conditions, with fixed values $M = 2$, $m = 2$, $\lambda = 2$, $\alpha = 0.9$, $h = 1$, $\sigma_{01} = 1.2$, $\sigma_{02} = 1.5$, $\varepsilon = 0.5$, $\rho = 1$, $\omega = 1$, $t = \pi / \omega$ and $s = 0.5$.

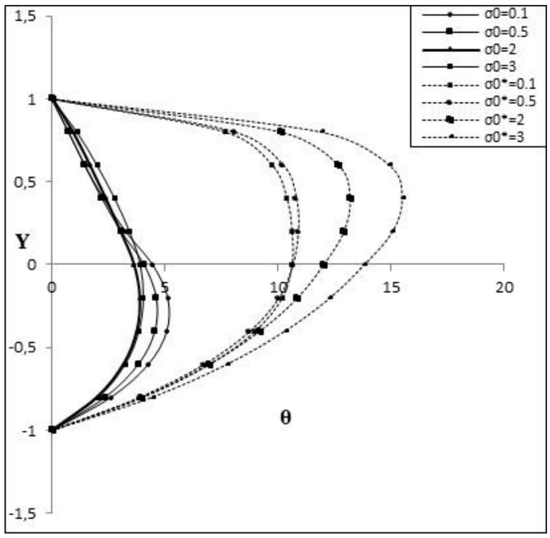

Fig.42. Effect of electrical conductivity ratio σ_0 on temperature components (θ_1, θ_2) for unsteady and (θ_1^*, θ_2^*) steady flow conditions, with fixed values $M = 4$, $m = 2$, $\lambda = 2$, $\alpha = 0.333$, $h = 0.75$, $\sigma_{01} = 1.2$, $\sigma_{02} = 1.5$, $\beta = 1$, $\varepsilon = 0.5$, $\rho = 1$, $\omega = 1$, $t = \pi / \omega$ and $s = 0.5$.

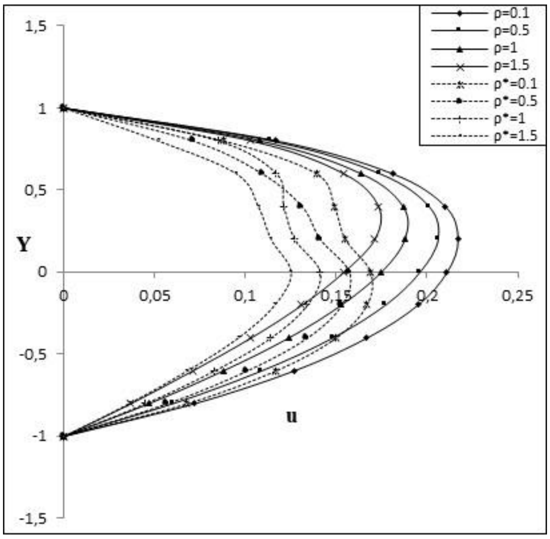

Fig.43. Effect of density ratio ρ on primary velocity components (u_1, u_2) for unsteady and (u_1^*, u_2^*) steady flow conditions, with fixed values $M=2$, $\alpha=0.9$, $m=2$, $\lambda=2$, $\sigma_0=1$, $\sigma_{01}=1.2$, $\sigma_{02}=1.5$, $\varepsilon=0.5$, $h=1$, $\omega=1$, $t=\pi/\omega$ and $s=0.5$.

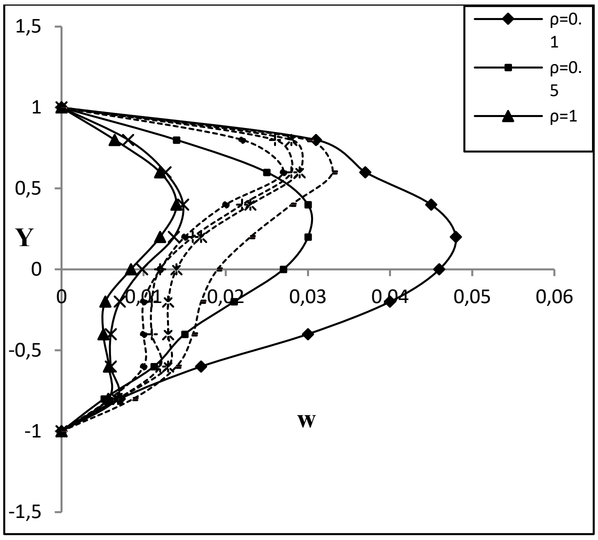

Fig.44. Effect of density ratio ρ on secondary velocity components (w_1, w_2) for unsteady and (w_1^*, w_2^*) steady flow conditions, with fixed values $M=2$, $\alpha=0.1$, $m=2$, $\lambda=2$, $\sigma_0=2$, $\sigma_{01}=1.2$, $\sigma_{02}=1.5$, $\varepsilon=0.5$, $h=1$, $\omega=1$, $t=\pi/\omega$ and $s=0.5$.

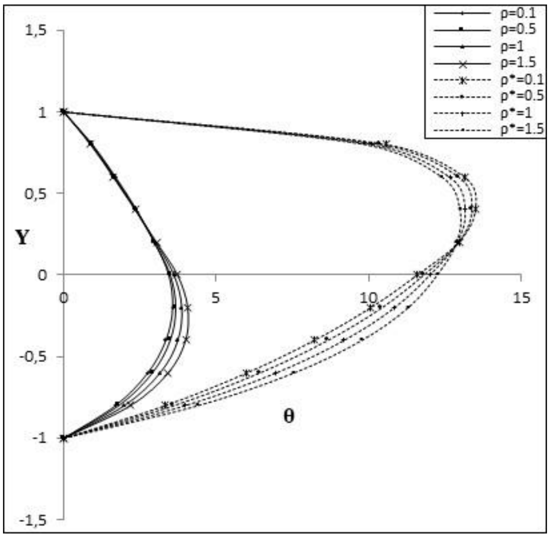

Fig.45. Effect of density ratio ρ on temperature components (θ_1, θ_2) for unsteady and (θ_1^*, θ_2^*) steady flow conditions, with fixed values $M=4$, $m=2$, $\lambda=2$, $\alpha=0.333$, $h=0.75$, $\sigma_0=2$, $\sigma_{01}=1.2$, $\sigma_{02}=1.5$, $\varepsilon=0.5$, $\beta=1$, $\omega=1$, $t=\pi/\omega$ and $s=0.5$.

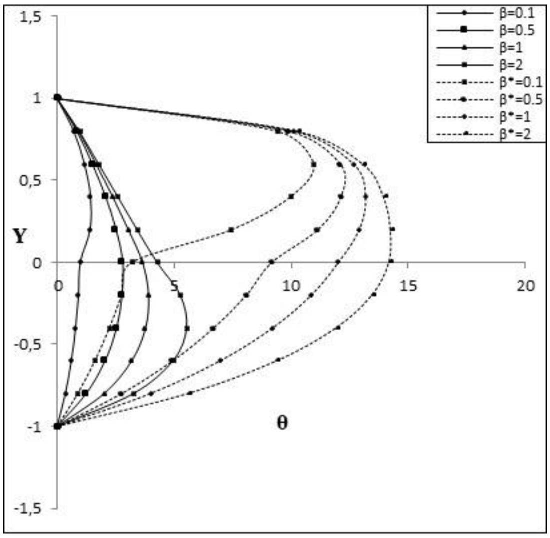

Fig.46. Effect of thermal conductivity ratio β on temperature components (θ_1, θ_2) for unsteady and (θ_1^*, θ_2^*) steady flow conditions, with fixed values $M=4$, $m=2$, $\lambda=2$, $\alpha=0.333$, $h=0.75$, $\sigma_0=2$, $\sigma_{01}=1.2$, $\sigma_{02}=1.5$, $\varepsilon=0.5$, $\rho=1$, $\omega=1$, $t=\pi/\omega$ and $s=0.5$.

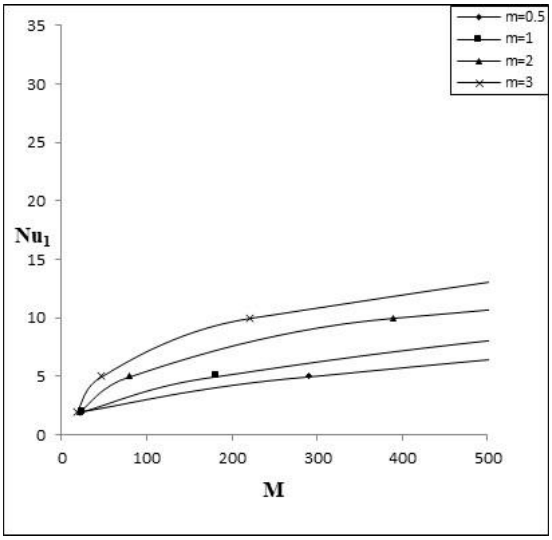

Fig.47. Variation of Nusselt number Nu_1 with different Hartmann number M values for fixed parameters $\alpha = 0.333$, $\sigma_0 = 2$, $\lambda = 1$, $\sigma_{01} = 1.2$, $\sigma_{02} = 1.5$, $\rho = 1$, $h = 0.75$, $\beta = 1$, $\varepsilon = 0.5$, $\omega = 1$, $t = \pi / \omega$ and $s = 0.5$.

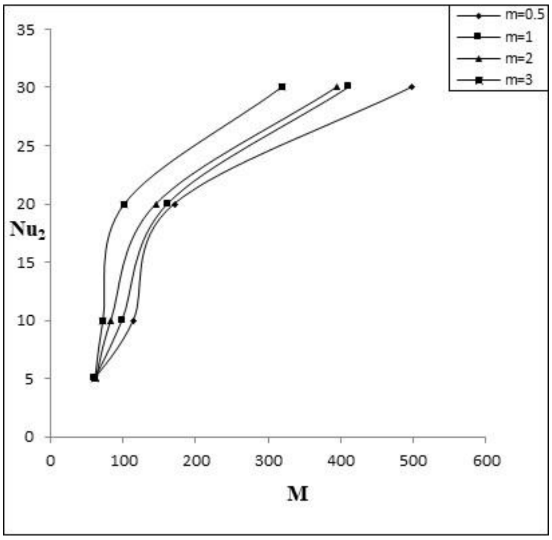

Fig.48. Variation of Nusselt number Nu_2 with different Hartmann number M values for fixed parameters $\alpha = 0.333$, $\sigma_0 = 2$, $\lambda = 1$, $\sigma_{01} = 1.2$, $\sigma_{02} = 1.5$, $\rho = 1$, $h = 0.75$, $\beta = 1$, $\varepsilon = 0.5$, $\omega = 1$, $t = \pi / \omega$ and $s = 0.5$.

In region-I, the fluid temperature increases progressively whereas in region-II, it initially drops as σ_0 reaches 2 before rising again beyond this point and the peak temperature moves beneath the centerline into region-II as σ_0 increases. This means that the electrical conductivity has a strong influence on both velocity and temperature because it alters the current density and the amount of Joule heating, redistributing energy between the regions.

The trend of primary, secondary flow velocities and temperature fields under varying density ratios ρ is illustrated in Figs 43-45. A rise in the density ratio causes a noticeable decline in the primary velocity within both fluid regions. In contrast, the secondary velocity reduces initially, attaining a minimum at $\rho = 1$, before rising afterward. The peak velocity shifts above the channel centerline toward region-I. Temperature trends show a decrease up to a specific point $\rho = 0.2$, followed by an increase in both regions with the maximum temperature moving beneath the central axis within region-II as the density ratio increases. That is, higher density makes the fluid harder to accelerate, reducing velocities throughout the channel.

Figure 46 illustrates how changes in the thermal conductivity ratio-β influence temperature distribution. With β increasing, temperature raises in both flow regions, and the maximum thermal level slightly moves downward toward region-II. That is, the greater thermal conductivity spreads heat more effectively, increasing overall temperatures and moving the peaks into region II.

Figures 47 and 48 reveal that, for $s = 1/2$ the heat transfer coefficients on both plates rise with increasing Hartmann number-M while holding other parameters constant. A further increase in the Hall parameter enhances this thermal transport at both boundaries.

In this configuration, total heat transfer increases with both Hartmann number M and Hall parameter m, as electromagnetic effects enhance mixing and energy exchange between the fluid and the boundaries.

5. Conclusions

This article examines unsteady ionized hydro magnetic two-fluids flow through a channel of conducting permeable side plates with heat transfer in the presence of Hall currents, aiming to extend existing

MHD models by incorporating the combined effects of unsteadiness, Hall currents and wall porosity. Temperature and velocity behaviors are studied in terms of electron pressure fraction. The analysis investigates the sensitivity of the flow and thermal characteristics to variations in parameters such as Hartmann number, Hall factor, fluid viscosities and densities, channel geometry, electrical conductivities, and thermal property ratios. Two distinct cases - one assuming zero ionization and the other considering half ionization - are analyzed, with a comparative discussion highlighting the significant differences in fluid motion and heat transfer between the two scenarios. The study holds significance for applications in aerospace, plasma physics, geophysics, and various industries such as chemical processing, petroleum, and power generation, with practical uses in reactor cooling, aerodynamic boundary layer control, spacecraft, MHD generators, pumps, flow meters, Hall accelerators, plasma jets.

For *s = 0* (electron-to-total pressure ratio):

1. Hartmann number effect – higher M reduces velocities and temperature, shifting peaks to region-I.
2. Hall parameter effect – increasing m raises velocities, lowers temperature up to $m = 2$, then increases, with peaks moving to region-I.
3. Porous parameter effect – alters velocities and temperature differently in regions I and II, with shifts in peak values.
4. Viscosity and height ratio effects – both increase velocities, shifting peaks, while temperature trends vary across regions.
5. Conductivity and heat transfer effects – thermal and electrical conductivity influence temperature distribution and peak shifts, with heat transfer rising with M and m.

For *s = 1/2* (electron-to-total pressure ratio):

1. Hartmann number effect – higher M reduces primary velocity but first increases, then decreases secondary velocity. Temperature drops, with peaks shifting to region-I.
2. Hall parameter effect – increasing m raises both velocities, shifting primary peak to region-I and secondary peak to region-II. Temperature declines, with peaks moving to region-II.
3. Porous and viscosity effects – both influence velocities and temperature differently across regions, with shifting peak values.
4. A rise in the height ratio modifies the flow speeds, whereas variations in electrical conductivity significantly influence both velocity and temperature distributions within the two regions.
5. Density and thermal conductivity effects – density reduces velocities, while thermal conductivity raises temperature, shifting peaks to region-II. Heat transfer rises with M and m.

Hence, from the above individual results, here's a comparative interpretation of how each parameter behaves when the electron-to-total pressure ratio changes from *s = 0* to *s = 1/2*:

Hartmann number:

At *s = 0*: Stronger magnetic fields slow the flow due to Lorentz force dominance, reducing both velocity and temperature. Peaks shift toward region I. Joule heating exists but is outweighed by the magnetic damping.

At *s = 1/2*: The primary velocity still decreases with stronger magnetic fields, but the secondary velocity first increases (due to altered cross-flow currents) before eventually decreasing. Temperature drops in both velocity components, with primary peaks shifting to region I and secondary peaks to region II.

Comparison: For $s = 1/2$, the secondary velocity shows a non-monotonic response to M, unlike at $s = 0$ where both velocities simply decline.

Hall parameter:

At $s = 0$: Increasing m weakens magnetic braking, causing velocities to rise and shifting peaks toward region I. Temperature first falls (better heat removal) until about $m \approx 2$, then rises due to reduced cooling efficiency.

At $s = 1/2$: Both primary and secondary velocities increase with m. The primary peak moves to region I, but the secondary peak shifts to region II. Temperature drops steadily, with heat transport concentrating in region II.

Comparison: At $s = 0$, temperature has a 'minimum–maximum trend' with m, whereas at $s = 1/2$, the drop is 'monotonic'. Secondary velocity shifts are also more pronounced at $s = 1/2$.

Porous parameter:

At $s = 0$: Changes in wall permeability can either increase or reduce velocities depending on region, altering peak positions for both velocity and temperature.

At $s = 1/2$: Similar competing effects occur, but the influence is more region-dependent, with stronger interactions between wall drag and momentum redistribution.

Comparison: The qualitative effect is similar for both cases, but $s = 1/2$ shows 'greater spatial variation' in the response.

Viscosity and height ratio:

At $s = 0$: Higher viscosity or changes in height ratio generally increase velocities and shift peaks; temperature response varies by region.

At $s = 1/2$: Viscosity effects are still strong, but geometric constraints from height ratio changes significantly alter the distribution of primary and secondary flows.

Comparison: Both show velocity shifts, but at $s = 1/2$, the geometry-viscosity interaction is 'more dominant' in redistributing flow.

Electrical conductivity:

At $s = 0$: Higher σ changes current paths and Joule heating, modifying flow and increasing heat transfer in combination with M and m.

At $s = 1/2$: Electrical conductivity strongly affects both velocity and temperature, redistributing energy more effectively between regions.

Comparison: At $s = 1/2$, electrical conductivity has a 'more uniform and pronounced' influence on overall energy distribution.

Thermal conductivity and density:

At $s = 0$: Higher Thermal conductivity smoothes temperature gradients; density effects are less emphasized.

At $s = 1/2$: Higher Thermal conductivity raises overall temperature and moves peaks to region II; higher density reduces velocities significantly.

Comparison: Thermal conductivity has a stronger role in $s = 1/2$, and density effects are explicitly important there but not highlighted for $s = 0$.

Limitations of the current work

This work provides useful understanding of how Hall currents and wall porosity affect transient MHD two-fluid heat transfer flow of ionized gases in a horizontal straight channel bounding two permeable plates.

However, it has some constraints. The study focuses on an idealized parallel-plate setup with a constant pressure gradient and assumes smooth, fully developed flow, leaving out possible complexities like turbulence, three-dimensional flow effects, or non-uniform magnetic fields. The use of the regular perturbation method limits the results to situations with small parameter changes, meaning strongly nonlinear or extreme cases are not captured. The analysis also assumes fixed material properties and simplified boundary conditions, without accounting for temperature-dependent variations often present in real applications. Moreover, only two ionization scenarios–no ionization and half ionization–are examined, so the behavior under full or variable ionization remains unknown. Addressing these gaps in future research through more realistic geometries, broader parameter ranges, advanced numerical modeling, and experimental validation could make the findings more applicable to engineering practice.

Use of software

In this study, Mathcad and MS Excel are used to plot graphs that illustrate the results and trends of key governing parameters. These visualizations help in interpreting the physical significance of the findings, showing how variations in parameters affect flow behavior and heat transfer characteristics.

Future scope of the problem

- The future scope involves extending the study of unsteady magneto hydrodynamic two-fluid flows of ionized gases with heat transfer in a horizontal channel between two parallel plates, influenced by a uniform transverse magnetic field and Hall effects in a rotating system.
- Also, the same can be extended in the slip flow regime either in parallel or vertical or inclined channel with or without permeable plates.

Acknowledgements

- The authors sincerely thank all the reviewers, and the Editor-In-Chief: Prof. Pawel Jurczak for their suggestions and support in improving the quality of this piece of our research work.
- The authors sincerely appreciate the valuable contributions of the researchers whose studies have been cited throughout this paper.

Financial support for research: NIL

This research was conducted without any financial support from any institutions (or) organization (or) government body (or) external funding source.

Nomenclature

$\left.\begin{array}{r} A_1, A_2, \ldots a_1, a_2, \ldots \\ B_1, B_2, \ldots b_1, b_2, \ldots \end{array}\right\}$ – symbols or functional expressions utilized within the governing equations and their respective solutions.

$\overline{B}$ – magnetic flux density $[T]$

B_0 – represents a uniform transverse magnetic field applied to the system $[A/m]$

E_x, E_z – denotes applied electric fields in the x- and z-directions, respectively $[V/m]$

e – symbol for electric charge $[C]$

h – ratio representing the relative heights of the two fluid regions.

h_1 – height of the upper channel region (Region-I)

h_2 – height of the lower channel region (Region-II)

$I_{x_1}, I_{z_1}; I_{x_2}, I_{z_2}$ – Non-dimensional current density components along the x- and z-axes for both fluid domains

J_x, J_z – current density components in the x- and z-directions, respectively
$\overline{J}$ – represents the total current density $\left[A/cm^2\right]$
K_1, K_2 – thermal conductivity values for the fluids in Region-I and Region-II $\left[W/(mK)\right]$
M – Hartmann number, indicating the influence of the magnetic field on the fluid flow
m – Hall parameter, describing the Hall effect's contribution to current density distribution $\left[m^2/C\right]$
$m_1, m_2, m_3, \ldots$ – additional mathematical symbols or functional expressions considered within the analytical framework
m_x, m_z – non-dimensional electric field components
N_1, N_2 – general symbols introduced for mathematical representation as $N_1 = m_{x_1} + im_{z_1}$ and $N_2 = m_{x_2} + im_{z_2}$
Nu_1, Nu_2 – heat transfer coefficients at the upper and lower plates, respectively $\left[W/\left(m^2 K\right)\right]$
P – pressure within the system $[Pa]$
p_e – pressure due to electrons $[Pa]$
Pr – Prandtl number, representing the ratio of momentum diffusivity to thermal diffusivity
$q_{01}, q_{02}, q_{11}, q_{12}$ – Application of complex notations for analytical convenience
q_{m_1}, q_{m_2} – complex expressions for the mean velocity profiles $[m/s]$
s – $= pe/p$ (ratio of electron pressure to the total fluid pressure)
t – time
T –temperature
T_{w_1}, T_{w_2} – constant temperatures maintained at the boundaries (plates)
U_1, U_2 – symbols adopted for simplification in equations as $U_1 = q_1/q_{m_1}$, $U_2 = q_2/q_{m_2}$
$\overline{U_1}, \overline{U_2}$ – complex conjugate of the associated variables U_1, U_2
u_1, u_2 – primary velocity profiles in the two distinct fluid regions
u_{m_1}, u_{m_2} – mean values of the primary velocity distributions in both fluid regions
$u_{01}(y), u_{02}(y)$ – steady-state primary velocity distributions within the two fluid domains
$u_{11}(y), u_{12}(y)$ – time-dependent (transient) components of primary velocity in the two regions
u_p – $\left(-\frac{\partial p}{\partial x}\frac{h_1^2}{\rho_1 \nu_1}\right)$: characteristic velocity scale
w_1, w_2 – secondary velocity profiles in the two fluid regions
w_{m_1}, w_{m_2} – mean values of the secondary velocity distributions in both regions
$w_{01}(y), w_{02}(y)$ – steady-state secondary velocity profiles in the two fluid domains
$w_{11}(y), w_{12}(y)$ – time-dependent (transient) secondary velocity components in the two regions
(x, y, z) – spatial coordinate variables
α – ratio of dynamic viscosities of the two fluids
λ –porous parameter characterizing the medium's permeability
β – ratio of thermal conductivities between the two fluids
μ_1, μ_2 – dynamic viscosities of the respective fluids $[Pa\ s]$
σ_0 – ratio of electrical conductivities between the two fluid regions
σ_1, σ_2 – modified electrical conductivities aligned parallel and normal to the electric field direction
σ_{01}, σ_{02} – electrical conductivities of the fluids in the two domains $[S/m]$
$\sigma_{11}, \sigma_{12}, \sigma_{21}, \sigma_{22}$ – adjusted conductivities in directions parallel and perpendicular to the electric field
ε – amplitude, typically representing a small constant value, $\varepsilon << 1$) $[m/s]$
ρ – ratio of fluid densities in the two regions
ρ_0 – free charge density within the fluid system $\left[C/m^2\right]$

ρ_1, ρ_2 – densities of the individual fluid regions $\left[kg/m^2\right]$

$\theta_1,\ \theta_2$ – non-dimensional temperature distribution in the two fluids

$\theta_{01}(y),\ \theta_{02}(y)$ – temperature distributions under steady-state conditions in both regions $[K]$

$\theta_{11}(y),\ \theta_{12}(y)$ – temperature distributions in the transient (time-dependent) state within both fluid domains

$\tau,\ \tau_e$ – mean collision time between electrons and ions or neutral particles

ω – non-dimensional frequency of oscillation in the system $[Hz]$

Appendix

$$\beta_1 = 1 - s\left(\frac{1}{1+m^2}\right),\quad \beta_2 = \frac{-sm}{1+m^2},\quad \beta_3 = 1 - s\left(1 - \frac{\sigma_0\sigma_{01}}{1+m^2}\right),\quad \beta_4 = \frac{-s\sigma_0\sigma_{02}m}{1+m^2},\quad D_1 = \beta_1 + i\beta_2,\quad D_2 = \beta_3 + i\beta_4,$$

$$D_3 = i\sigma_1 + m\sigma_2,\quad N_1 = m_{1x} + im_{1z},\quad N_2 = m_{2x} + im_{2z},\quad c_1 = M^2\left(\frac{mi-1}{1+m^2}\right),\quad c_2 = -\left(f_9 + M^2 N_1\left(\frac{i+m}{1+m^2}\right)\right),$$

$$c_3 = -\left(\frac{1}{1+m^2}\right)\alpha h^2 M^2\left(\sigma_1 - mi\sigma_2\right),\quad c_4 = -\left(f_{10}\alpha h^2 + \left(\frac{1}{1+m^2}\right)\alpha h^2 M^2 N_2\left(i\sigma_1 + m\sigma_2\right)\right),\quad c_{97} = \frac{e^{f_{30}} - 1}{f_{30}},$$

$$c_{98} = \frac{e^{f_{31}} - 1}{f_{31}},\quad c_{99} = \frac{e^{f_{32}} - 1}{f_{32}},\quad c_{100} = \frac{e^{f_{33}} - 1}{f_{33}},\quad d_{23} = f_{30} + \overline{f_{30}},\quad d_{24} = f_{30} + \overline{f_{31}},\quad d_{25} = f_{31} + \overline{f_{30}},$$

$$d_{26} = f_{31} + \overline{f_{31}},\quad d_{27} = d_5 + d_9,\quad d_{28} = d_6 + d_{10},\quad d_{29} = d_7 + d_{12},\quad d_{30} = d_8 + d_{13},\quad d_{31} = d_{11} + d_{20},$$

$$d_{31} = d_{14} + d_{21},\quad d_{33} = d_{15} + d_{18},\quad d_{34} = d_{16} + d_{19},\quad d_{35} = d_{17} + d_{22} + d_1 d_4 d_2,\quad d_{36} = \frac{d_{27}}{d_{23}{}^2 + \lambda d_{23}},$$

$$d_{37} = \frac{d_{28}}{d_{24}{}^2 + \lambda d_{24}},\quad d_{38} = \frac{d_{29}}{d_{25}{}^2 + \lambda d_{25}},\quad d_{39} = \frac{d_{30}}{d_{26}{}^2 + \lambda d_{26}},\quad d_{45} = \lambda\rho\alpha h,$$

$$d_{73} = d_{56}\frac{c_4}{c_3}\frac{\overline{c_4}}{\overline{c_3}} - d_{54}d_{56}\frac{c_4}{c_3} - d_{56}d_{53}\frac{\overline{c_4}}{\overline{c_3}} + d_{56}d_{53}d_{54},\quad d_{74} = f_{32} + \overline{f_{32}},\quad d_{75} = f_{32} + \overline{f_{33}},\quad d_{76} = f_{33} + \overline{f_{32}},$$

$$d_{77} = f_{33} + \overline{f_{33}},\quad d_{78} = d_{57} + d_{61},\quad d_{79} = d_{58} + d_{62},\quad d_{80} = d_{59} + d_{64},\quad d_{81} = d_{60} + d_{65},\quad d_{82} = d_{63} + d_{71},$$

$$d_{83} = d_{66} + d_{72},\quad d_{84} = d_{67} + d_{79},\quad d_{85} = d_{68} + d_{70},\quad d_{86} = \frac{d_{78}}{d_{74}^2 + d_{45}d_{74}},\quad d_{87} = \frac{d_{79}}{d_{75}^2 + d_{45}d_{75}},$$

$$d_{88} = \frac{d_{80}}{d_{76}^2 + d_{45}d_{76}},\quad d_{89} = \frac{d_{81}}{d_{77}^2 + d_{45}d_{77}},\quad d_{120} = \frac{d_{114}}{d_{113}},\quad d_{134} = d_{123}\overline{f_5},\quad d_{135} = d_{123}\overline{f_6},$$

$$d_{137} = d_{124} + f_6,\quad d_{138} = f_{34} + \overline{f_{34}},\quad d_{139} = f_{34} + \overline{f_{35}},\quad d_{140} = f_{35} + \overline{f_{34}},\quad d_{141} = f_{35} + \overline{f_{35}},$$

$$d_{142} = d_{126} + d_{130},\quad d_{143} = d_{127} + d_{131},\quad d_{144} = d_{128} + d_{132},\quad d_{145} = d_{129} + d_{133},\quad d_{185} = f_{36} + \overline{f_{36}},$$

$$d_{186} = f_{36} + \overline{d_{37}},\quad d_{187} = f_{37} + \overline{f_{36}},\quad d_{188} = f_{37} + \overline{f_{37}},\quad d_{189} = d_{173} + d_{177},\quad d_{190} = d_{174} + d_{178},$$

$$d_{191} = d_{175} + d_{179},\quad d_{192} = d_{176} + d_{180},\quad d_{200} = \frac{d_{182}}{\left(\overline{f_{37}}\right)^2 + d_{45}\overline{f_{37}} + d_{120}},\quad d_{232} = \frac{d_{227}}{f_{30}^2 + \lambda f_{30}},$$

$$d_{233}=\frac{d_{228}}{f_{31}^2+\lambda f_{31}},\quad d_{234}=\frac{d_{229}}{\left(\overline{f_{30}}\right)^2+\lambda\overline{f_{30}}},\quad d_{235}=\frac{d_{230}}{\left(\overline{f_{31}}\right)^2+\lambda\overline{f_{31}}},\quad d_{252}=\frac{d_{247}}{f_{33}^2+d_{45}f_{33}},$$

$$d_{253}=\frac{d_{248}}{\left(\overline{f_{32}}\right)^2+d_{45}\overline{f_{32}}},\quad d_{254}=\frac{d_{249}}{\left(\overline{f_{33}}\right)^2+d_{45}\overline{f_{33}}},\quad d_{255}=\frac{d_{250}}{d_{45}},\quad d_{289}=\frac{d_{285}}{d_{138}^2+\lambda d_{138}+d_{120}},$$

$$d_{290}=\frac{d_{286}}{d_{139}^2+\lambda d_{139}+d_{120}},\quad d_{291}=\frac{d_{287}}{d_{140}^2+\lambda d_{140}+d_{120}},\quad d_{292}=\frac{d_{288}}{d_{141}^2+\lambda d_{141}+d_{120}},$$

$$d_{293}=\frac{d_{281}}{\left(\overline{f_{34}}\right)^2+\lambda f_{30}+d_{120}},\quad d_{294}=\frac{d_{282}}{\left(\overline{f_{35}}\right)^2+\lambda f_{35}+d_{120}},\quad d_{295}=\frac{d_{283}}{f_{34}^2+\lambda f_{34}+d_{120}},$$

$$d_{296}=\frac{d_{284}}{f_{35}^2+\lambda f_{35}+d_{120}},\quad d_{315}=\frac{d_{311}}{d_{185}^2+d_{45}d_{185}+d_{120}},\quad d_{316}=\frac{d_{312}}{d_{186}^2+d_{45}d_{186}+d_{120}},$$

$$d_{317}=\frac{d_{313}}{d_{187}^2+d_{45}d_{187}+d_{120}},\quad d_{318}=\frac{d_{314}}{d_{188}^2+d_{45}d_{188}+d_{120}},\quad d_{319}=\frac{d_{307}}{\left(\overline{f_{36}}\right)^2+d_{45}\overline{f_{36}}+d_{120}},$$

$$d_{320}=\frac{d_{308}}{\left(\overline{f_{37}}\right)^2+d_{45}\overline{f_{37}}+d_{120}},\quad d_{321}=\frac{d_{309}}{f_{36}{}^2+d_{45}f_{36}+d_{120}},\quad d_{322}=\frac{d_{310}}{f_{37}{}^2+d_{45}f_{37}+d_{120}},$$

$$f_1=c_{53}c_{13}+c_{54}c_{16},\quad f_2=c_6-f_1e^{c_5},\quad f_3=c_{73}c_{13}+f_1c_{74},\quad f_4=c_8-f_3e^{c_7},\quad f_5=f_{24},$$

$$f_6=f_{15}+f_5f_{16},\quad f_7=f_8f_{18},\quad f_8=f_{25},\quad f_{28}=\varepsilon\cos\omega t\left(f_{24}\left(\frac{e^{f_{34}}-1}{f_{34}}\right)+f_{26}\left(\frac{e^{f_{35}}-1}{f_{35}}\right)\right),$$

$$f_{29}=\varepsilon\cos\omega t\left(f_{27}\left(\frac{e^{f_{36}}-1}{f_{36}}\right)+f_{25}\left(\frac{e^{f_{37}}-1}{f_{37}}\right)\right),\quad f_{30}=\frac{\lambda+\sqrt{\lambda^2-4c_1}}{2},\quad f_{31}=\frac{\lambda-\sqrt{\lambda^2-4c_1}}{2},$$

$$f_{32}=\frac{\lambda_1+\sqrt{\lambda_1{}^2-4c_3}}{2},\quad f_{33}=\frac{\lambda_1-\sqrt{\lambda_1{}^2-4c_3}}{2},\quad f_{34}=\frac{\lambda+\sqrt{\lambda^2-4(c_1+\omega\tan\omega t)}}{2},$$

$$f_{35}=\frac{\lambda-\sqrt{\lambda^2-4(c_1+\omega\tan\omega t)}}{2},\quad f_{36}=\frac{\lambda_1+\sqrt{\lambda_1{}^2-4(c_3+\omega\tan\omega t)}}{2},\quad g_9=\frac{-\lambda+\sqrt{\lambda^2-4d_{120}}}{2},$$

$$f_{37}=\frac{\lambda_1-\sqrt{\lambda_1{}^2-4(c_3+\omega\tan\omega t)}}{2},\quad g_{10}=\frac{-\lambda-\sqrt{\lambda^2-4d_{120}}}{2},\quad g_{11}=\frac{-d_{45}+\sqrt{d_{45}^2-4d_{120}}}{2},$$

$$g_{12}=\frac{-d_{45}-\sqrt{d_{45}^2-4d_{120}}}{2},\quad g_{13}=d_{267},\quad g_{14}=d_{266},\quad g_{15}=d_{268},\quad g_{16}=d_{265},\quad g_{17}=d_{335},$$

$$g_{18}=d_{334},\quad g_{19}=d_{336},\quad g_{20}=d_{333}.$$

References

[1] Hartmann J. (1937): *Theory of the laminar flow of an electrically conductive liquid in a homogeneous magnetic field.*– Math. Fys. Dan. Vid. Selsk., vol.15, No.6, pp.1-28.

[2] Siegel R. (1958): *Effect of magnetic field on forced convection heat transfer in a parallel plate channel.*– J. Appl. Mech., vol.25, No.3, pp.415-416, https://doi.org/10.1115/1.4011841.

[3] Nigam S.D. and Singh S.N. (1960): *Heat transfer by laminar flow between parallel plates under the action of transverse magnetic fields.*– Quart. J. Mech. Appl. Math., vol.13, No.1, pp.85-97, https://doi.org/10.1093/qjmam/13.1.85.

[4] Alpher R.A. (1961): *Heat transfer in magnetohydrodynamic flow between parallel plates.*– Int. J. Heat Mass Transf., vol.3, No.2, pp.108-112, https://doi.org/10.1016/0017-9310(61)90073-4.

[5] Shercliff J.A. (1962): *The Theory of Electromagnetic Flow Measurement.*– Cambridge University Press, New York.

[6] Singh K.R. and Cowling T.G. (1963): *Thermal convection in magnetohydrodynamics. Part II, Flow in rectangular box.*– Quart. J. Mech. Appl. Math., vol.16, No.1, pp.17-31, https://doi.org/10.1093/qjmam/16.1.17.

[7] Alireza S. and Sahai V. (1990): *Heat transfer in developing magnetohydrodynamic Poiseuille flow and variable transport properties.*– Int. J. Heat Mass Transf., vol.33, No.8, pp.1711-1720, https://doi.org/10.1016/0017-9310(90)90026-Q.

[8] Morley N.B., Malang S. and Kirillov I. (2005): *Thermo-fluid magnetohydrodynamic issues for liquid breeders.*– Fusion Sci. Technol., vol.47, pp.488-501, https://doi.org/10.13182/FST05-A733.

[9] Selimli S.Z. and Resebli E. (2015): *Combined effects of magnetic and electric field on hydrodynamic and thermo physical parameters of magneto viscous fluid flow.*– Int. J. Heat Mass Transf., vol.86, pp.426-432, https://doi.org/10.1016/j.ijheatmasstransfer.2015.03.003.

[10] Jovanovic M.M., Nikodijevic J.D. and Nikodijevic M.D. (2015): *Rayleigh–Bénard convection instability in the presence of spatial temperature modulation on both plates.*– Int. J. Non-Linear Mech., vol.73, pp.69-74, https://doi.org/10.1016/j.ijnonlinmec.2014.11.017.

[11] Hsiao K.L. (2017): *Combined electrical MHD heat transfer thermal extrusion system using Maxwell fluid with radiative and viscous dissipation effects.*– Appl. Therm. Eng., vol.112, pp.1281-1288, https://doi.org/10.1016/j.applthermaleng.2016.08.208.

[12] Nikodijevic M., Stamenkovic Z., Petrovic J. and Kocic M. (2020): *Unsteady fluid flow and heat transfer through a porous medium in a horizontal channel with an inclined magnetic field.*– Trans. FAMENA, vol.44, No.4, pp.31-46, https://doi.org/10.21278/TOF.444014420.

[13] Das D., Shaw S., Mondal K.K. and Kairi R.R. (2023): *Analyzing the impact of boundary slip and absorption effects on the dispersion of solute in a pulsatile channel flow of Casson fluid under magnetic field.*– Eur. Phys. J. Plus, vol.138, art.372, https://doi.org/10.1140/epjp/s13360-023-03973-8.

[14] Sadab M. and Kundu S. (2025): *Study of Love waves in a nonlocal piezoelectric plate induced by a point source using FDA and Green's function derivatives.*– J. Eng. Mech., vol.151, No.8, https://doi.org/10.1061/JENMDT.EMENG-8130.

[15] Sadab M. and Kundu S. (2025): *Dispersive wave propagation in piezoelectric–piezomagnetic imperfectly bonded media with surface effects based on strain gradient theory.*– Mech. Res. Commun., vol.145, art.104390, https://doi.org/10.1016/j.mechrescom.2025.104390.

[16] Sherman A. and Sutton G.W. (1961): *Magnetohydrodynamics.*– Evanston, Illinois, p.123.

[17] Sato H. (1961): *The Hall effect in the viscous flow of ionized gas between parallel plates under transverse magnetic field.*– J. Phys. Soc. Jpn., vol.16, No.1, pp.1427-1433, https://doi.org/10.1143/JPSJ.16.1427.

[18] Romig M.F. (1964): *The influence of electric and magnetic fields on heat transfer to electrically conducting fluids.*– Advances in Heat Transfer, vol.1, Academic Press, New York, pp.268-352, https://doi.org/10.1016/S0065-2717(08)70100-X.

[19] Jana R.N. and Datta N. (1977): *Hall effects on hydromagnetic flow over an impulsively started porous plate.*– Acta Mech., vol.28, pp.211-218, https://doi.org/10.1007/BF01208799.

[20] Mandal G. and Mandal K.K. (1983): *Effect of Hall current on MHD Couette flow between thick arbitrarily conducting plates in a rotating system.*– J. Phys. Soc. Jpn., vol.52, No.1, pp.470-477, https://doi.org/10.1143/JPSJ.52.470.

[21] Sharma R.C. and Rani N. (1988): *Hall effects of thermo-solute instability of a plasma.*– Indian J. Pure Appl. Math., vol.19, No.2, pp.202-207.

[22] LingaRaju T. and RamanaRao V.V. (1993): *Hall effects on temperature distribution in a rotating ionized hydromagnetic flow between parallel walls.*– Int. J. Eng. Sci., vol.31, No.7, pp.1073-1091, https://doi.org/10.1016/0020-7225(93)90117-X.

[23] Attia H.A. (1998): *Hall current effects on the velocity and temperature fields of an unsteady Hartmann flow*.– Can. J. Phys., vol.76, No.9, pp.739-746.

[24] Takhar H.S., Chamkha A.J. and Nath G. (2002): *MHD flow over a moving plate in a rotating fluid with magnetic field, Hall currents and free stream velocity.*– Int. J. Eng. Sci., vol.40, No.13, pp.1511-1527.

[25] Ghosh S.K., Beg O.A. and Narahari M. (2009): *Hall effects on MHD flow in a rotating system with heat transfer characteristics.*– Meccanica, vol.44, No.6, pp.741-765, DOI:10.1007/s11012-009-9210-6.

[26] Hazem A.A. (2009): *Effect of Hall current on the velocity and temperature distribution of Couette flow with variable properties and uniform suction and injection*.– Comput. Appl. Math., vol.28, No.2, pp.195-212.

[27] Jha B.K. and Apere C.A. (2010): *Combined effects of Hall and ion-slip currents on unsteady MHD Couette flows in a rotating system.*– J. Phys. Soc. Jpn., vol.79, No.10, art.104401.

[28] Pal D., Talukdar B., Shivakumara I.S. and Vajravelu K. (2012): *Effects of Hall current and chemical reaction on oscillatory mixed convection radiation of a micropolar fluid in a rotating system*.– Chem. Eng. Commun., vol.199, No.8, pp.943-965, https://doi.org/10.1080/00986445.2011.628318.

[29] Siddiqa S., Hossain M.A. and Subba Reddy G.R. (2013): *Hall current effects on magnetohydrodynamic natural convection flow with strong cross magnetic field.*– Int. J. Thermal Sci., vol.71, pp.196-204, https://doi.org/10.1016/j.ijthermalsci.2013.04.016.

[30] Makinde O.D., Iskander T., Mabood F., Khan W.A. and Tshehla M.S. (2016): *MHD Couette-Poiseuille flow of variable viscosity nanofluids in a rotating permeable channel with Hall effects*.– J. Mol. Liq., vol.221, pp.778-787, https://doi.org/10.1016/j.molliq.2016.06.037.

[31] Rashidi M.M. and Momoniat E. (2020): *Effects of Hall and ion-slip currents on MHD free convection flow of a nanofluid over a stretching sheet.*– Alexandria Eng. J., vol.59, No.5, pp.3561-3570.

[32] Gorla R.S.R. and Gupta A.K. (2020): *Effects of Hall current and rotation on MHD natural convection flow past an impulsively moving vertical plate with ramped temperature in the presence of thermal diffusion with heat absorption.*– Int. J. Energy Technol., vol.5, No.16, pp.1-12.

[33] Das S. and Deka R.K. (2021): *Effects of Hall current and rotation on unsteady MHD Couette flow with heat transfer in a porous medium.*– J. Appl. Fluid Mech., vol.14, No.1, pp.239-250.

[34] Alam M. (2022): *Unsteady MHD fluid flow over an inclined plate with Hall and ion-slip currents in an inclined magnetic field.*– Rend. Circ. Mat. Palermo, vol.71, No.3, pp.175-192, https://DOI:10.1007/s11587-022-00728-y.

[35] Matao P., Reddy B.P. and Sunzu J. (2022): *Hall and rotation effects on radiating and reacting MHD flow past an accelerated permeable plate with Soret and Dufour effects.*– Trends Sci., vol.19, No.5, art.2618.

[36] Hossain M.A. and Alim M.A. (2022): *Impact of Hall current, Dufour and Soret on transient MHD flow past an impulsively started vertical plate in a porous medium*.– J. King Saud Univ. Sci., vol.34, No.2, art.101912.

[37] LingaRaju T. and Satish P. (2023): *MHD two liquid plasma heat transfer flow with Hall current between parallel plates.*– Int. J. Appl. Mech. Eng., vol.28, No.3, pp.65-85, https://doi.org/10.59441/ijame/172898.

[38] Ramesh K. and Ojjela O. (2025): *Entropy generation analysis of mixed convective Eyring-Powell nanofluid flow with Hall and ion slip effects.*– Z. Angew. Math. Mech., vol.105, art.e202400863, https://doi.org/10.1002/zamm.202400863.

[39] Shrestha G.M. (1967): *Singular perturbation problems of laminar flow in a uniformly porous channel in the presence of a transverse magnetic field.*– Quart. J. Mech. Appl. Math., vol.20, No.2, pp.233-246, https://doi.org/10.1093/qjmam/20.2.233.

[40] Ockendon H. and Ockendon J.R. (1977): *Variable-viscosity flows in heated and cooled channels.*– J. Fluid Mech., vol.83, No.1, pp.177-190.

[41] Debnath L., Ray S.C. and Chatterjee A.K. (1979): *Effect of Hall current on hydromagnetic flow past a porous plate in a rotating fluid system.*– Z. Angew. Math. Mech., vol.59, pp.469-471.

[42] Attia H.A. and Sayed-Ahmed M.E. (2002): *A transient Hartmann flow with heat transfer of a non-Newtonian fluid with suction and injection, considering the Hall effect.*– J. Plasma Phys., vol.67, No.1, pp.27-47.

[43] Attia H.A. (2007): *Velocity and temperature distributions between parallel porous plates with Hall effect and variable properties.–* Chem. Eng. Commun., vol.194, No.10, pp.1355-1373, https://doi.org/10.1080/00986440701401487.

[44] Ganesh S. and Krishnambal S. (2007): *Unsteady magnetohydrodynamic Stokes flow of viscous fluid between two parallel porous plates.–* J. Appl. Sci., vol.7, No.3, pp.374-379, DOI:10.3923/jas.2007.374.379.

[45] Ahmed N. and Goswami J.K. (2011): *Hall effect on MHD forced convection from an infinite porous plate with dissipative heat in a rotating system.–* Turk. J. Phys., vol.35, pp.293-302.

[46] Manyonge W.A., Kiema D.W. and Iyaya W.C.C. (2012): *Steady MHD Poiseuille flow between two infinite parallel porous plates in an inclined magnetic field.–* Int. J. Pure Appl. Math., vol.76, No.5, pp.661-668.

[47] Das S., Mandal H.K. and Jana R.N. (2013): *Hall effects on unsteady rotating MHD flow through a porous channel with variable pressure gradient.–* Int. J. Comput. Appl., vol.83, No.1, pp.7-18, https://doi.org/10.5120/14418-2519.

[48] Jaber K.K. (2015): *Influence of Hall current and viscous dissipation on MHD convective heat and mass transfer in a rotating porous channel with Joule heating.–* Amer. J. Math. Stat., vol.5, No.5, pp.272-284, https://doi.org/10.5923/j.ajms.20150505.08.

[49] Singh J.K., Begum S.G. and Seth G.S. (2018): *Influence of Hall current and wall conductivity on hydromagnetic mixed convective flow in a rotating Darcian channel.–* Phys. Fluids, vol.30, art.013602, https://doi.org/10.1063/1.5054654.

[50] Akinshilo A.T. (2018): *Flow and heat transfer of nanofluid with injection through an expanding or contracting porous channel under magnetic force field.–* Eng. Sci. Technol. Int. J., vol.21, pp.486-494, https://doi.org/10.1016/j.jestch.2018.03.014.

[51] Veera Krishna M., Swarnalathamma B.V. and Chamkha A.J. (2019): *Investigation of Soret, Joule and Hall effects on MHD rotating mixed convective flow past an infinite vertical porous plate.–* Journal of Ocean Engineering and Science, vol.4, No.3, pp.263-275, https://doi.org/10.1016/j.joes.2019.05.002.

[52] Nayak M.K., Mahanta G., Das M. and Shaw S. (2022): *Entropy analysis of a 3D nonlinear radiative hybrid nanofluid flow between two parallel stretching permeable sheets with slip velocities.–* International Journal of Ambient Energy, vol.43, No.1, pp.8710-8721, https://doi.org/10.1080/01430750.2022.2101523.

[53] Vangala G.S.R. and LingaRaju T. (2024): *The influence of Hall currents on unsteady MHD heat transfer flow in a conducting channel containing two ionized fluids.–* Int. J. Appl. Mech. Eng., vol.29, No.3, pp.118-149, DOI:10.59441/ijame/187212.

[54] Lohrasbi J. and Sahai V. (1988): *Magnetohydrodynamic heat transfer in two phase flow between parallel plates.–* Appl. Sci. Res., vol.45, No.1, pp.53-66, https://doi.org/10.1007/BF00384182.

[55] Malashetty M.S. and Leela V. (1992): *Magnetohydrodynamic heat transfer in two phase flow.–* Int. J. Eng. Sci., vol.30, No.3, pp.371-377, https://doi.org/10.1016/0020-7225(92)90082-R.

[56] Chamkha A.J. (2004): *Unsteady MHD convective heat and mass transfer past a semi-infinite vertical permeable moving plate with heat absorption.–* Int. J. Eng. Sci., vol.42, No.2, pp.217-230, https://doi.org/10.1016/S0020-7225(03)00285-4.

[57] Sharma R.C. and Rani N. (1986): *Finite Larmor radius and compressibility effects on thermosolutal instability of a plasma.–* Z. Naturforsch. A, vol.41, No.5, pp.724-728, https://doi.org/10.1515/zna-1986-0505.

[58] Sharma R.C. and Rani N. (1989): Thermosolutal instability of a plasma in the presence of a porous medium and Hall currents.– Astrophys. Space Sci., vol.151, No.1, pp.51-58, https://doi.org/10.1007/BF00645162.

[59] LingaRaju T. and Seedhar S. (2009): *Unsteady two-fluid flow and heat transfer of conducting fluids in channels under transverse magnetic field.–* Int. J. Appl. Mech. Eng., vol.14, No.4, pp.1093-1114.

[60] Kalra G.L., Kathuria S.N., Hosking R.J. and Lister G.G. (1970): *Effect of Hall current and resistivity on the stability of a gas liquid system.–* J. Plasma Phys., vol.4, No.3, pp.451-469, https://doi.org/10.1017/S0022377800005158.

[61] Packham B.A. and Shail R. (1971): *Stratified laminar flow of two immiscible fluids.–* Proc. Camb. Phil. Soc., vol.69, No.3, pp.443-448.

[62] Shail R. (1973): *On laminar two-phase flows in magnetohydrodynamics.–* Int. J. Eng. Sci., vol.11, No.10, pp.1103-1108, .

[63] Shikhmurzaev Y.D. (1993): *A two-layer model of an interface between immiscible fluids.–* Physica A, vol.192, No.1-2, pp.47-62.

[64] Vajravelu K., Arunachalam P.V. and Sreenadh S. (1995): *Unsteady flow of two immiscible conducting fluids between two permeable beds.–* J. Math. Anal. Appl., vol.196, No.3, pp.1105-1126, https://10.1006/jmaa.1995.1463.

[65] Umavathi J.C., Mateen A., Chamkha A.J. and Al-Mudhaf A. (2006): *Oscillatory Hartmann two-fluid flow and heat transfer in a horizontal channel.*– Int. J. Appl. Mech. Eng., vol.11, No.1, pp.155-178.

[66] Ozen O., Li F., Aubry N., Papageorgiou D.T. and Petropoulos P.G. (2007): *Linear stability of two-fluid interface for electrohydrodynamic mixing in a channel.*– J. Fluid Mech., vol.583, pp.347-377.

[67] Murthy J.R. and Srinivas J. (2013): *Second law analysis for Poiseuille flow of immiscible micropolar fluids in a channel.*– Int. J. Heat Mass Transf., vol.65, pp.254-264, https://doi.org/10.1016/j.ijheatmasstransfer.2013.05.048.

[68] LingaRaju T. and Naga Valli M. (2014): *MHD two-layered unsteady fluid flow and heat transfer through a horizontal channel between parallel plates in a rotating system.*– Int. J. Appl. Mech. Eng., vol.19, No.1, pp.97-121, https://doi.org/10.2478/ijame-2014-0008.

[69] Sharma P.R. and Sharma K. (2014): *Unsteady MHD two-fluid flow and heat transfer through a horizontal channel.*– Int. J. Eng. Sci. Invention Res. Dev., vol.1, No.3, pp.65-72.

[70] Sivakamini L. and Govindarajan A. (2019): *Unsteady MHD flow of two immiscible fluids under chemical reaction in a horizontal channel.*– AIP Conf. Proc., vol.2112, art.020157, pp.1-9, https://doi.org/10.1063/1.5112342.

[71] AbdElmaboud Y., Abdesalam S.I., Mekheimer K.S. and Vafai K. (2019): *Electromagnetic flow for two-layer immiscible fluids.*– Eng. Sci. Technol. Int. J., vol.22, No.1, pp.237-248, https://doi.org/10.1016/j.jestch.2018.07.018.

[72] Roy A.K. and Shaw S. (2021): *Shear augmented micro vascular solute transport with a two-phase model: Application in nano particle assisted drug delivery.*– Phys. Fluids, vol.33, No.3, art.031904, https://doi.org/10.1063/5.0035754.

[73] LingaRaju T. and Satish P. (2023): *Hall and rotation effects on magnetohydrodynamics two fluids slip flow of ionized gases via parallel conduit.*– Heat Transfer, vol.52, No.7, pp.4829-4856, https://doi.org/10.1002/htj.22909.

[74] LingaRaju T. and Naga Valli M. (2023): *Effect of Hall currents on the EMHD two-layered plasma heat transfer flow via a channel of porous plates.*– J. Eng. Phys. Thermophys., vol.96, No.5, pp.1278-1289, https://doi.org/10.1007/s10891-023-02794-x.

[75] Kalra G.L., Kathuria S.N., Hosking R.J. and Lister G.G. (1970): *Effect of Hall current and resistivity on the stability of a gas-liquid system.*– J. Plasma Phys., vol.4, No.3, pp.451-469, https://doi.org/10.1017/S0022377800005158.

[76] LingaRaju T. (2019): *MHD heat transfer two-ionized fluids flow between two parallel plates with Hall currents.*– Results Eng., vol.4, art.100043, pp.1-15, https://doi.org/10.1016/j.rineng.2019.100043.

[77] Srinivasacharya D. and Kaladhar K. (2020): *Unsteady magnetohydrodynamic flow of generalized second grade fluid through a porous medium with Hall effects on heat and mass transfer.*– Phys. Fluids, vol.32, No.11, art.113105, https://doi.org/10.1063/5.0023946.

[78] Spitzer L. Jr. (1956): *Physics of Fully Ionized Gases.*– Interscience Publishers, New York.

[79] Nayak M.K., Shaw S., Waqas H., Makinde O.D., Alghamdi M. and Muhammad T. (2021): *Comparative study for magnetized flow of nanofluids between two parallel permeable stretching/shrinking surfaces.*– Case Stud. Therm. Eng., vol.28, art.101353, https://doi.org/10.1016/j.csite.2021.101353.

[80] Sadab M. and Kundu S. (2024): *An analytical model for Love wave in a coated piezoelectric bar via nonlocal theory due to an impulsive source.*– Eur. J. Mech. A Solids, vol.107, art.105372, https://doi.org/10.1016/j.euromechsol.2024.105372.

[81] LingaRaju T. and VenkatRao B. (2022): *Unsteady electro-magneto hydrodynamic flow and heat transfer of two ionized fluids in a rotating system with Hall currents.*– Int. J. Appl. Mech. Eng., vol.27, No.1, pp.125-145, https://doi.org/10.2478/ijame-2022-0009.

Received: June 30, 2025
Revised: March 19, 2026